

# Rates and Characteristics of Intermediate Mass Ratio Inspirals Detectable by Advanced LIGO

Ilya Mandel

*Theoretical Astrophysics, California Institute of Technology, Pasadena, CA 91125;  
Department of Physics and Astronomy, Northwestern University, Evanston, IL 60208*

ilyamandel@chgk.info

Duncan A. Brown

*LIGO Laboratory, California Institute of Technology, Pasadena, CA 91125;  
Theoretical Astrophysics, California Institute of Technology, Pasadena, CA 91125;  
Department of Physics, Syracuse University, Syracuse, NY 13244*

Jonathan R. Gair

*Institute of Astronomy, Madingley Road, Cambridge, CB3 0HA, UK*

and

M. Coleman Miller

*University of Maryland, Department of Astronomy, College Park, MD 20742*

## ABSTRACT

Gravitational waves (GWs) from the inspiral of a neutron star (NS) or stellar-mass black hole (BH) into an intermediate-mass black hole (IMBH) with mass  $M \sim 50M_{\odot}$  to  $350M_{\odot}$  may be detectable by the planned advanced generation of ground-based GW interferometers. Such intermediate mass ratio inspirals (IMRIs) are most likely to be found in globular clusters. We analyze four possible IMRI formation mechanisms: (1) hardening of an NS–IMBH or BH–IMBH binary via three-body interactions, (2) hardening via Kozai resonance in a hierarchical triple system, (3) direct capture, and (4) inspiral of a CO from a tidally captured main-sequence star; we also discuss tidal effects when the inspiraling object is an NS. For each mechanism we predict the typical eccentricities of the resulting IMRIs. We find that IMRIs will have largely circularized by the time they enter the sensitivity band of ground-based detectors. Hardening of a binary via three-body interactions, which is likely to be the dominant mechanism for

IMRI formation, yields eccentricities under  $10^{-4}$  when the GW frequency reaches 10 Hz. Even among IMRIs formed via direct captures, which can have the highest eccentricities, around 90% will circularize to eccentricities under 0.1 before the GW frequency reaches 10 Hz. We estimate the rate of IMRI coalescences in globular clusters and the sensitivity of a network of three Advanced LIGO detectors to the resulting GWs. We show that this detector network may see up to tens of IMRIs per year, although rates of one to a few per year may be more plausible. We also estimate the loss in signal-to-noise ratio that will result from using circular IMRI templates for data analysis and find that, for the eccentricities we expect, this loss is negligible.

*Subject headings:* black hole physics — globular clusters: general — gravitational waves

## 1. Introduction

Observational evidence from cluster dynamics and from ultra-luminous X-ray sources suggests that there may exist a population of intermediate-mass black holes (IMBHs) with masses in the  $M \sim 10^2 - 10^4 M_\odot$  range (Miller & Colbert 2004; Trenti 2006). Numerical simulations of globular clusters suggest that IMBHs could merge with numerous lower-mass compact objects (COs) during the lifetime of the cluster (Taniguchi et al. 2000; Miller & Hamilton 2002a,b; Mouri & Taniguchi 2002a,b; Gültekin, Miller, & Hamilton 2004, 2006; O’Leary et al. 2006; O’Leary, O’Shaughnessy, & Rasio 2007), through a combination of emission of gravitational radiation, binary exchange processes, and secular evolution of hierarchical triple systems. Gravitational waves (GWs) will be generated during the intermediate-mass-ratio inspiral (IMRI) of a stellar-mass object (black hole [BH] or neutron star [NS], since a white dwarf or a main-sequence star would be tidally disrupted) into an IMBH. For IMBH mass  $\lesssim 350 M_\odot$ , these waves are potentially detectable with the planned advanced generation of ground-based GW interferometers: Advanced LIGO and its international partners (Barish & Weiss 1999; Fritschel 2003).

IMRIs will be important as probes of strong gravity and cluster dynamics due to their mass range and dynamical histories. For example, from Advanced LIGO IMRI data it may be possible to measure the quadrupole moment,  $Q$ , of an IMBH to an accuracy of  $\Delta Q \sim Q_{\text{Kerr}}$ , where  $Q_{\text{Kerr}}$  is the quadrupole moment of a Kerr BH (Brown et al. 2007). This is sufficient to distinguish a BH from a boson star, for which the quadrupole moment can be many times the Kerr value. In addition, since the formation of IMBHs in clusters seems to require short mass segregation timescales (see § 2), detection of IMBH mergers and their associated masses

will yield information about young dense clusters and their evolution.

In this paper we discuss the astrophysical and data analysis aspects of IMRIs. In § 2 we provide the astrophysical setting for IMRIs and describe the formation mechanisms. We estimate the typical eccentricities resulting from different capture mechanisms and find that inspirals will largely circularize by the time the GW frequency reaches the Advanced LIGO band ( $f_{\text{GW}} \gtrsim 10$  Hz). We show, in particular, that three-body hardening, which is likely to be the dominant IMRI formation mechanism, will result in binary eccentricities  $e < 10^{-4}$  in the Advanced LIGO band. Even direct capture, which is the most likely mechanism to yield high eccentricities, leads to  $\sim 90\%$  of IMRIs with  $e < 0.1$  in the Advanced LIGO band. In § 3 we estimate an upper limit on the rate of IMRIs detectable by Advanced LIGO of up to 10 events per year. A more sophisticated, but model-dependent, rate estimate ranges from one event per 3 years for NS IMRIs to 10 events per year for  $10 M_{\odot}$  BH IMRIs. The event rate can be enhanced by a factor of  $\sim 3.5$  by optimizing Advanced LIGO for detections at low frequencies.<sup>1</sup> Searches for IMRIs in Advanced LIGO data will likely use matched filtering techniques, for which accurate waveform templates are required. In § 4, we estimate that there will be a negligible loss in signal-to-noise ratio (S/N) if circular templates are used to search for IMRIs with the expected eccentricities in Advanced LIGO data.

## 2. Astrophysical Setting, Capture Mechanisms, and Typical Eccentricities

An IMBH cannot result from the evolution of a solitary star in the current universe because even a star of initial mass  $\sim 10^2 M_{\odot}$  will be reduced well below this mass by winds and pulsational instabilities driven by metal-line opacities (cf. Fryer & Kalogera (2001), Fig. 7 and associated discussion). Some IMBHs might be formed from the first, metal-free, stars (Madau & Rees 2001), but these IMBHs are unlikely to participate in multiple mergers with COs. Instead, we focus on the proposal that IMBHs can be produced in the current universe via runaway stellar collisions in dense young stellar clusters. If the most massive stars segregate to the center in less than their  $\sim 2 \times 10^6$  yr lifetimes (Ebisuzaki et al. 2001; Portegies Zwart & McMillan 2002; Portegies Zwart et al. 2004; Gürkan, Freitag, & Rasio 2004; Gürkan, Fregeau, & Rasio 2006; Freitag, Rasio, & Baumgardt 2006; Freitag, Gürkan, & Rasio 2006; Fregeau et al. 2006), then stellar mergers can overcome mass losses and the collision product can reach hundreds to thousands of solar masses, presumably evolving into an IMBH.

When supernovae start to occur, the resulting mass loss leads to an expansion of the

---

<sup>1</sup>We used the Advanced LIGO Bench code to perform this optimization: <http://www.ligo.mit.edu/bench/bench.html>

cluster, which thus transitions into a more collisionless stage of existence. From this point on, COs can be captured by the IMBH and generate observable GWs as they inspiral under radiation reaction and eventually merge with the IMBH.

Early in the history of the globular cluster the inspiraling objects in IMRIs are likely to be  $m \sim 10 M_{\odot}$  BHs, which may form a dense subcluster composed purely of BHs around the IMBH (O’Leary et al. 2006; O’Leary, O’Shaughnessy, & Rasio 2007). Late in the cluster’s history, once the BH central subcluster has largely evaporated, NSs will likely replace the larger BHs as the inspiraling objects.

There are several ways in which stellar-mass COs can be captured by an IMBH. Most mechanisms of capture involve binaries, because the cross section of a binary is orders of magnitude larger than that of a single CO.

Extensive numerical studies of binary-single interactions demonstrate that hard binaries (defined, e.g., so that the total energy of the binary-single system is negative) tend to be tightened by three-body interactions (Heggie 1975). These studies also show that massive objects such as stellar-mass BHs and IMBHs tend to swap into binaries. The most likely capture mechanism involves the formation of a CO–IMBH binary, which is subsequently hardened by repeated three-body interactions until radiation reaction becomes significant and the binary coalesces.

Hardening can also occur via binary-binary interactions; unlike binary-single interactions, these can result in a stable hierarchical triple. Some fraction of these end up in orientations favorable for the secular Kozai resonance (Kozai 1962), in which the inner binary (which contains the IMBH) periodically increases and decreases its eccentricity while keeping its semimajor axis constant. The periapsis distance can therefore be quite low in parts of the cycle and can lead to coalescence without Newtonian recoil (Miller & Hamilton 2002b; Wen 2002), although recoil from gravitational radiation will still occur (see § 3.2). The importance of the Kozai resonance depends on the frequency of binary-binary interactions, which is unknown at present.

In addition to these mechanisms, which usually require multiple interactions to lead to merger, a hyperbolic encounter at a close enough periapsis can produce direct capture via emission of gravitational radiation. Assuming that the IMBH does not have a significant radius of influence, the effective cross section for radiative capture of the CO by an IMBH is proportional to  $M^{12/7}$ , where  $M$  is the mass of the IMBH (Quinlan & Shapiro 1987). For two-body encounters this process is likely to be important only for masses high enough ( $\gtrsim 10^3 M_{\odot}$ ) that the frequency of the GWs throughout the subsequent inspiral will be below the sensitivity range of ground-based detectors. However, direct capture during a three-body

interaction could be significant (Gültekin, Miller, & Hamilton 2006).

Finally, an IMBH could tidally capture a main-sequence star. If the captured star evolves to a CO while in orbit around the IMBH, the remnant could remain bound to the IMBH and ultimately spiral in via GW emission. This scenario has been suggested as a possible explanation for the observed population of ultraluminous X-ray sources (Hopman, Portegies Zwart, & Alexander 2004; Hopman & Portegies Zwart 2005).

Additionally, orbital energy may couple to vibrational normal modes of the inspiraling object in the case when the inspiraling object is an NS. In principle, the energy loss to tidal heating of an NS could change the inspiral trajectory, or even disrupt the NS.

The IMRI enters the Advanced LIGO band when

$$f_{\text{GW}} = \frac{\omega_{\text{orb}}(r_p)}{\pi} = \frac{1}{\pi} \sqrt{\frac{M}{r_p^3}} \gtrsim 10 \text{ Hz}, \quad (1)$$

i.e., when the periapsis is  $r_p \approx 16GM/c^2 = 1600GM_\odot/c^2$  for  $M = 100M_\odot$ . The frequency of the dominant quadrupolar ( $k = 2$ ) harmonic in the GWs emitted at the innermost stable circular orbit is

$$f_{\text{GW, ISCO}} \approx 44.0 \frac{M}{100 M_\odot} \text{ Hz} \quad (2)$$

for inspirals into non-spinning BHs.

Below, we discuss the eccentricity of an IMRI at the time its GW frequency enters the Advanced LIGO band for each of the mechanisms mentioned above: (1) formation of a CO–IMBH binary and subsequent hardening via three-body interactions, (2) Kozai resonance of a hierarchical triple system, (3) direct capture when a solitary CO passes close to the IMBH, and (4) tidal capture of a main-sequence star that subsequently evolves to leave a CO. We also consider the impact of (5) tidal interactions with an inspiraling NS.

## 2.1. Hardening of a CO–IMBH Binary via Three-Body Interactions

This mechanism proceeds as follows. The IMBH rapidly swaps into a binary because it is far more massive than any other object in the globular cluster. Advanced LIGO can detect IMRIs at redshifts  $z \lesssim 0.2$  (§ 3.1), so it will predominantly observe globular clusters late in their history. On a timescale that is short relative to the merger time, an NS or a BH will encounter the binary containing the IMBH and will exchange for the companion in this binary, since stellar remnants are the most massive objects in the late cluster other than the IMBH itself. From that point on, stars of all types (although biased towards the

heavy ones that segregate towards the center) engage in three-body interactions. Numerical simulations show that interactions tend to tighten a binary if it is hard. This can be understood heuristically for three equal-mass objects by noting that ejection will tend to occur at roughly the binary orbital speed; hence, if this is greater than the initial encounter speed at infinity the binary loses energy. Binary tightening proceeds until the binary can merge through radiation reaction from the emission of GWs.

For the unequal mass binaries we consider here, simulations by Quinlan (1996) show that a single interaction of a field star of mass  $m_*$  with a binary of total mass  $M$  will on average change the binary energy by a fractional amount  $\Delta E/E = \mathcal{O}(m_*/M)$ , roughly independent of the component masses of the binary. More precisely, approximately  $(2\pi/22)M/m_*$  interactions are required to reduce the semimajor axis of a hard binary by one  $e$ -folding (Quinlan 1996).

The rate at which objects interact with the IMBH binary is

$$\dot{N} = n\zeta v, \quad (3)$$

where  $n$  is the number density,  $v$  is the relative speed, and  $\zeta$  is the gravitationally focused cross section  $\zeta = \pi a(2GM/v^2)$  for an interloper to approach within the binary's semimajor axis  $a$  of the binary. Since this rate is proportional to  $a$ , the total time for the binary to harden until the semimajor axis equals  $a$  is dominated by the last  $e$ -folding time:

$$T_{\text{harden}} \approx \frac{2\pi}{22} \frac{M}{m_*} \frac{1}{\dot{N}} \approx 2 \times 10^8 \left( \frac{10^{13} \text{ cm}}{a} \right) \text{ yr}, \quad (4)$$

where we set  $m_* = 0.5 M_\odot$ ,  $v = 10^6 \text{ cm s}^{-1}$ , and  $n = 10^{5.5} \text{ pc}^{-3}$  (the number density of all stars in a core-collapsed globular cluster; Pryor & Meylan 1993).

For a sufficiently massive BH, a cusp is formed and the interactions are no longer described by individual binary-single encounters. We can estimate roughly the mass above which this occurs. Consider a core of number density  $n_{\text{core}}$  and velocity dispersion  $\sigma$ . For an IMBH of mass  $M$ , the radius of influence (inside of which the IMBH dominates the potential) is  $r_{\text{infl}} = GM/\sigma^2$ . For a true cusp, Bahcall & Wolf (1976) showed that the number density would go as  $n(r) = n_{\text{core}}(r/r_{\text{infl}})^{-7/4}$ . The total number of objects inside  $r_{\text{infl}}$  is then

$$N(r < r_{\text{infl}}) = \int_0^{r_{\text{infl}}} 4\pi r^2 n_{\text{core}} (r/r_{\text{infl}})^{-7/4} dr = (16\pi/5) r_{\text{infl}}^3 n_{\text{core}}. \quad (5)$$

Scaling to canonical values, this gives

$$N(r < r_{\text{infl}}) \approx 0.3(M/100 M_\odot)^3 (\sigma/10 \text{ km s}^{-1})^{-6} (n_{\text{core}}/10^{5.5} \text{ pc}^{-3}) \quad (6)$$

Therefore, in the mass range most relevant to Advanced LIGO, it is unlikely that there will be a significant cusp, hence our treatment of isolated binary-single interactions is reasonable. For more massive BHs a cusp might form, although we note that for  $M < 1000 M_\odot$  the typical distance wandered by the IMBH in the core is larger than the radius of influence; hence, cusp formation could be made more difficult. This is, however, worth further study.

The gravitational radiation merger timescale for an intermediate-mass-ratio binary of semimajor axis  $a$ , eccentricity  $e$ , reduced mass  $\mu \approx m$ , and total mass approximately equal to the IMBH mass  $M$ , is (Peters 1964)

$$T_{\text{merge}} \approx 10^{17} \frac{M_\odot^3}{M^2 m} \left( \frac{a}{10^{13} \text{ cm}} \right)^4 (1 - e^2)^{7/2} \text{ yr.} \quad (7)$$

Simulations and phase-space arguments show that three-body interactions cause the eccentricity of the binary to sample a thermal distribution  $P(e)de = 2ede$  (Heggie 1975) in the Newtonian realm where gravitational radiation is not significant. If an interaction leaves the binary with a high eccentricity, however, it is more likely to merge. Gültekin, Miller, & Hamilton (2006) examined the eccentricity of the binary after its final three-body encounter and found a typical value of  $e \approx 0.98$  due to this bias. Taking this as the typical value for eccentricity, we find

$$T_{\text{merge}} \approx 10^8 \left( \frac{M_\odot}{m} \right) \left( \frac{100 M_\odot}{M} \right)^2 \left( \frac{a}{10^{13} \text{ cm}} \right)^4 \text{ yr.} \quad (8)$$

In fact, there is a distribution of eccentricities after the last encounter, rather than a single eccentricity value of 0.98. However, Monte Carlo simulations, which are described below, confirm the typical merger times and final eccentricities computed here analytically by assuming the final-encounter eccentricity of 0.98. Moreover, simulations indicate that the fraction of direct plunges from highly radial orbits must be extremely small, because they would require improbably small periapsis separations.

The IMRI rate will be maximized when the total merger time,  $T = T_{\text{harden}} + T_{\text{merge}}$ , is minimized. Minimizing  $T$  with respect to  $a$ , we find that the total merger time is  $T \approx 3 \times 10^8$  yr for the inspiral of an  $m = 1.4 M_\odot$  NS into an  $M = 100 M_\odot$  IMBH, yielding an IMRI rate per globular cluster of  $\sim 3 \times 10^{-9} \text{ yr}^{-1}$ . If the inspiraling object is an  $m = 10 M_\odot$  BH, and the IMBH mass is again  $M = 100 M_\odot$ , then the total merger time is  $T \approx 2 \times 10^8$  yr, and the IMRI rate per globular cluster is  $\sim 5 \times 10^{-9} \text{ yr}^{-1}$ .

These numbers are close to the answers obtained with Monte Carlo simulations using the same procedure as in Gültekin, Miller, & Hamilton (2006). We find from these simulations that the total time to merger averages  $5 \times 10^8$  yr for  $1.4 M_\odot$  NSs and  $3 \times 10^8$  yr for  $10 M_\odot$  BHs, interacting with field stars of mass  $0.5 M_\odot$  and an IMBH of mass  $100 M_\odot$ . We also find

that, as we assumed, once a CO is in a binary with an IMBH it stays there; only a fraction  $\approx 6 \times 10^{-4}$  of encounters swapped out an NS, and only 1 of the  $5 \times 10^4$  encounters swapped out a BH. Therefore, as we indicated, the object that eventually merges with the IMBH is highly likely to be a CO.

This mechanism requires the cluster to be in a core-collapsed state and for this state to persist for a time  $\gg 2 \times 10^8$ yr. Core collapse is expected to persist in the absence of significant heating, as will be the case for clusters with IMBHs in the mass range of interest, so  $2 \times 10^8$ yr should be easily achievable. About 20% of clusters currently are in a state of core collapse, so this state can indeed be sustained for times of order a Hubble time, or much longer than  $2 \times 10^8$ yr. We consider only these core-collapsed systems as likely hosts of IMRIs when computing event rates below.

Radiation reaction from GW emission dominates the evolution once the GW merger timescale  $T_{\text{merge}}$  [Eq. (8)] is shorter than the average time between three-body encounters,  $1/\dot{N}$ , defined by Eq. 3. For the NS–IMBH system ( $m = 1.4 M_\odot$ ,  $M = 100 M_\odot$ ), this occurs when the semimajor axis takes the value  $a \approx 5 \times 10^{12}$  cm. As discussed earlier, the eccentricity at this time is  $e \approx 0.98$ , and hence the periapsis is  $r_p \approx 10^{11}$  cm  $\approx 7000 GM/c^2$ . For the BH–IMBH system ( $m = 10 M_\odot$ ,  $M = 100 M_\odot$ ), radiation reaction dominates for  $a \lesssim 8 \times 10^{12}$  cm, corresponding to a periapsis of  $r_p \approx 1.6 \times 10^{11}$  cm  $\approx 10000 GM/c^2$ .

Keplerian orbits evolving under radiation reaction satisfy [see Eq. (5.11) of Peters (1964)]

$$r_p e^{-12/19}(1+e) \left[1 + (121/304)e^2\right]^{-870/2299} = \text{constant}, \quad (9)$$

from which we can obtain the eccentricity at a particular frequency, given the initial values of periapsis and eccentricity. We find that for this capture mechanism, the eccentricity when the source enters the Advanced LIGO band ( $f_{\text{GW}} = 10$  Hz) is very small:  $e \lesssim 3 \times 10^{-5}$  for the NS–IMBH system and  $e \lesssim 2 \times 10^{-5}$  for the BH–IMBH system. The orbit will thus have circularized by the time the IMRI is in the Advanced LIGO band. This is consistent with the results of Gültekin, Miller, & Hamilton (2006), who also found that IMRI binaries formed through this channel would circularize before they entered the Advanced LIGO band.

## 2.2. Kozai Resonance

A stable hierarchical triple system could experience Kozai resonance that would drive the eccentricity of the inner binary to a value close to unity (Kozai 1962), leading to a small periapsis separation and binary tightening and eventual merger through gravitational radiation reaction (Miller & Hamilton 2002b; Wen 2002). Some simulations (e.g., those

of O’Leary et al. (2006)) suggest that the four-body (binary-binary) interactions that are required to place the binary on the Kozai merger track constitute only a small fraction of the total number of merger events in the cluster. If so, four-body interactions play a minor role in IMRI formation. These simulations may not consider all possibilities, however. In particular, in the O’Leary et al. (2006) model, binaries are only destroyed (through mergers, or by being kicked out of the subcluster). Therefore, the binary fraction decreases with time, meaning that binary-binary interactions are uncommon late in the cluster’s history. There may be a way to replenish the number of BHs in binaries, however. Approximately 5%–20% of normal stars in globulars are in binaries (Rubenstein & Bailyn 1997; Bellazzini et al. 2002) (this fraction is closer to 50%–70% in the field, but in globulars the wide binaries are disrupted). If such a binary goes through the BH subcluster, a BH could swap in, so that even if no BHs were originally in binaries, the binary fraction could increase.

Although computing the relative contribution of Kozai resonance mergers to the total number of IMRIs requires more detailed modeling of the cluster dynamics, it is possible to estimate the largest eccentricity that could result from this mechanism (see Wen (2002) for a more detailed discussion in the context of stellar-mass BHs). For this calculation, we assume that the Kozai resonance drives the binary to a sufficiently high eccentricity to allow merger via radiation reaction within one Kozai cycle. In reality, the semimajor axis and eccentricity would evolve gradually over multiple Kozai cycles, leading to larger typical periapses and smaller eccentricities, so our assumption will overestimate the typical eccentricities of IMRIs in the Advanced LIGO band.

We assume that the eccentricity is near its maximum for a fraction 0.01 of the total Kozai cycle (based on Fig. 1 of Innanen et al. (1997)) and compare this time with the radiation reaction timescale. If the radiation reaction merger time is much longer than the time near maximum eccentricity, we assume that gravitational radiation is insignificant. If instead the timescale for Kozai resonance to drive the eccentricity to some value  $e \approx 1$  is much larger than the timescale for radiation reaction to circularize the orbit down from  $e$ , then the eccentricity will never reach  $e$  in practice, even though  $e$  may be less than the maximum possible eccentricity for the given configuration (see below). Therefore, the maximum eccentricity reachable when including gravitational radiation is given approximately by the condition that the radiation reaction timescale is equal to the time near that high eccentricity.

The timescale for the Kozai cycle is given by, e.g., Eq. (4) of Miller & Hamilton (2002b):

$$\tau_{\text{Kozai}} \approx \text{few} \times \left( \frac{M_1 b_2^3}{m_2 a_1^3} \right)^{1/2} \left( \frac{b_2^3}{G m_2} \right)^{1/2} \approx 3 \times \left( \frac{M_1}{100 M_\odot} \right)^{1/2} \left( \frac{M_\odot}{m_2} \right) \left( \frac{b_2}{a_1} \right)^3 \left( \frac{a_1}{10^{13} \text{ cm}} \right)^{3/2} \text{ yr}, \quad (10)$$

where, in the notation of Miller & Hamilton (2002b),  $M_1$  is the total mass (approximately equal to the mass of the IMBH),  $m_1$  is the mass of the inner companion,  $m_2$  is the mass of the outer companion,  $a_1$  is the semimajor axis of the inner binary, and  $b_2$  is the semiminor axis of the outer binary. Setting the timescale for merger by gravitational radiation, given in Eq. (7), equal to  $\tau_{\text{GR}} = 0.01 \tau_{\text{Kozai}}$  yields

$$\left(\frac{a_1}{10^{13} \text{ cm}}\right)^{5/2} \epsilon^{7/2} \approx 3 \times 10^{-15} \left(\frac{M_1}{100 M_\odot}\right)^{5/2} \left(\frac{m_1}{m_2}\right) \left(\frac{b_2}{a_1}\right)^3 \quad (11)$$

where  $\epsilon \equiv 1 - e^2$ .

Relativistic precession constrains the maximal eccentricity, or minimal  $\epsilon$ , that can be achieved in a Kozai cycle. That minimal  $\epsilon$  is given by Eqs. (6) and (8) of Miller & Hamilton (2002b) as:

$$\epsilon \approx \frac{1}{9} \left(8 \frac{b_2^3 G M_1^2}{m_2 a_1^4 c^2}\right)^2 \approx 1.6 \times 10^{-7} \left(\frac{m_2}{M_\odot}\right)^{-2} \left(\frac{M_1}{100 M_\odot}\right)^4 \left(\frac{a_1}{10^{13} \text{ cm}}\right)^{-2} \left(\frac{b_2}{a_1}\right)^6. \quad (12)$$

In order to compute the maximal plausible eccentricity at  $f_{\text{GW}} = 10$  Hz, we need to estimate the minimal periapsis radius at the peak of the Kozai cycle, when radiation reaction becomes dominant, since eccentricity will be close to unity there [cf. Eq. (9)]. That is, we must minimize  $r_p = a_1(1 - e) \approx a_1\epsilon/2$ . This minimum value is found by solving Eqs. (11) and (12). We find

$$\frac{a_1 \epsilon}{10^{13} \text{ cm}} \gtrsim 1.8 \times 10^{-5} \left(\frac{m_2}{M_\odot}\right)^{-4/9} \left(\frac{M_1}{100 M_\odot}\right)^{13/9} \left(\frac{b_2}{a_1}\right)^2 \left(\frac{m_1}{m_2}\right)^{2/9}. \quad (13)$$

Stability requires that the semiminor axis of the outer binary is at least a few times greater than the semimajor axis of the inner binary, so we set  $b_2/a_1 = 5$ . We again assume  $M_1 = 100 M_\odot$ ,  $m_1 = 1.4 M_\odot$ , and  $m_2 = M_\odot$  (although this choice violates the restricted three-body assumption under which Eq. (8) of (Miller & Hamilton 2002b) was derived). These parameter values predict a minimal  $r_p \gtrsim 170 GM/c^2$  at the time when radiation reaction takes over; hence, according to Eq. (9), the maximal eccentricity of IMRIs formed via the Kozai resonance mechanism in the Advanced LIGO band is  $e \approx 0.01$ .

### 2.3. Direct Captures

If we assume that the IMBH is wandering in the stellar cluster, the effective cross section for direct captures via two-body relaxation (GW emission) is proportional to the

(12/7) power of the total mass (Quinlan & Shapiro 1987), so an IMBH has a relatively small capture cross section, making this capture mechanism relatively unlikely. If we instead assume that the  $M - \sigma$  relation holds for globular clusters, which is equivalent to saying that the IMBH dominates the dynamics in the center of the cluster, the capture rate would increase towards smaller IMBH masses, like  $M^{-1/4}$  (Hopman & Alexander 2005), and this channel would contribute significantly to the total rate. However, as discussed in § 2.1, the IMBHs of interest for Advanced LIGO, with  $M \sim 100M_\odot$ , have a very small radius of influence and so they will not have a significant influence on the dynamics in the cluster center. The direct capture mechanism, in any case, can yield higher eccentricities than scenarios involving binaries.

The critical periapsis separation  $r_p$  for the direct capture of a CO of mass  $m$ , moving at infinity with velocity  $v$ , by an IMBH of mass  $M \gg m$  is [e.g. Eq. (11) of Quinlan & Shapiro (1989)]:

$$\frac{r_p^{\max} c^2}{GM} \approx 950 \left(\frac{m}{M}\right)^{2/7} \left(\frac{v}{10^6 \text{ cm s}^{-1}}\right)^{-4/7}. \quad (14)$$

If  $M = 100 M_\odot$ ,  $m = 1.4 M_\odot$ , and  $v = 10^6 \text{ cm s}^{-1}$ , direct capture is possible at a maximum periapsis of  $r_p^{\max} c^2 / (GM) \approx 280$ ; if  $m = 10 M_\odot$  and  $M$  and  $v$  are the same as above, the maximum periapsis is  $r_p^{\max} c^2 / (GM) \approx 500$ . For such small periapses, gravitational focusing implies  $r_p \propto b^2$ , where  $b$  is the impact parameter. Hence, the probability distribution  $P(b) \propto b$  in impact parameter corresponds to a uniform distribution in periapsis at capture,  $P(r_p) = \text{constant}$ .

In Figure 1, we plot the eccentricity of an IMRI at the frequency at which it enters the Advanced LIGO band as a function of the initial periapsis at capture, following Eq. (9). The initial eccentricity at capture can be computed from the energy lost during the first pass; however, the exact value does not significantly affect the eccentricity at  $f_{\text{GW}} = 10$  Hz, so we set the eccentricity at capture to be  $e = 1$ . The initial periapsis is uniformly distributed between  $r_p^{\min} = 4GM/c^2$  (orbits with periapsis under  $4GM/c^2$  will plunge rather than inspiral) and  $r_p^{\max}$ . Therefore, to determine the total fraction of directly captured IMRIs that circularize to a given level  $e \leq e_{\text{cutoff}}$  by the time they are in the detector band, it is sufficient to find the fraction of the interval  $[r_p^{\min}, r_p^{\max}]$  for which the line in Fig. 1 stays below  $e_{\text{cutoff}}$ .

Thus, for the chosen IMBH mass of  $M = 100 M_\odot$ , if the CO is an  $m = 1.4 M_\odot$  NS, 86% of all directly captured IMRIs will be circularized to  $e \leq 0.1$  by the time they are in the Advanced LIGO band. If the CO is an  $m = 10 M_\odot$  BH, 92% of all directly captured IMRIs will be circularized to  $e \leq 0.1$  and 67% will be circularized to  $e \leq 0.01$  by the time they are in the detector band.

## 2.4. Tidal Capture of a Main-Sequence Star

It has been suggested that ultraluminous X-ray (ULX) sources are systems in which a main-sequence star that has been tidally captured is transferring mass to an IMBH via Roche lobe overflow (Hopman, Portegies Zwart, & Alexander 2004). In such a system, after the star reaches the end of its main-sequence lifetime and undergoes a supernova, it may leave a CO on an orbit about the IMBH (Hopman & Portegies Zwart 2005) and this object may then spiral into the IMBH via GW emission. Although work on this problem has focused on sources that might be detected by LISA, results have also been presented for the  $\sim 100M_{\odot}$  IMBHs that we consider here. For  $M \sim 100M_{\odot}$ , only 1%–2% of systems leave a CO that inspirals into the IMBH within a Hubble time, and these remnants are always NSs (Hopman & Portegies Zwart 2005). Following Hopman & Portegies Zwart (2005) we can estimate the rate of these events by assuming that there is  $\sim 1$  ULX source in each galaxy. The ULX phase lasts approximately the main-sequence lifetime of the captured star, which is  $\sim 10^7$  yr, so we estimate that the capture rate is  $10^{-7}$  yr $^{-1}$ . Multiplying by the fraction of events that successfully inspiral, we estimate a rate of  $1\text{--}2 \times 10^{-9}$  IMRIs per galaxy per year. There are typically  $\sim 100$  globular clusters per galaxy, so the rate per globular cluster is  $\sim 10^{-11}$  yr $^{-1}$ , which is considerably smaller than the binary hardening rate. Thus, while this channel could lead to some IMRIs detectable by Advanced LIGO, the rate is likely to be significantly lower than the binary hardening channel.

An NS captured via this mechanism would begin to inspiral into the IMBH with eccentricity  $e \lesssim 0.9$  (Hopman & Portegies Zwart 2005) and periapsis approximately equal to the tidal radius,  $(M/M_*)^{1/3}R_*$ , where  $M_* \gtrsim 10M_{\odot}$  and  $R_*$  are, respectively, the mass and radius of the main-sequence star. Assuming, conservatively,  $R_* \gtrsim 10^5$ km, this capture periapsis is typically  $\gtrsim 500(GM/c^2)$ . For an  $M = 100M_{\odot}$  IMBH, equation (9) predicts  $e \approx 0.002$  when the source enters the Advanced LIGO band. In practice, the eccentricity is likely to be even smaller. It is thus quite clear that this capture mechanism also produces sources that are essentially circular when they enter the Advanced LIGO band.

## 2.5. Tidal Effects

If the inspiraling object is an NS, tides may be significantly excited as it passes the central IMBH. If sufficient energy goes into tidal heating, the NS could be disrupted. Prior to disruption the orbital inspiral will be modified as orbital energy and angular momentum are lost into tidal heating. Tidal interactions are not important for the IMRI events we are considering, however, as we demonstrate below.

### 2.5.1. Tidal Disruption

A star will be tidally disrupted by a BH when the gravitational tidal force acting over the star due to the BH exceeds the self-gravity of the star. Assuming a Newtonian potential, this leads to the usual tidal disruption radius

$$R_{\text{td}} = R_* \left( \frac{M}{m} \right)^{\frac{1}{3}} = 41.5 \text{km} \left( \frac{R_*}{10 \text{km}} \right) \left( \frac{M/100M_\odot}{m/1.4M_\odot} \right)^{\frac{1}{3}}, \quad (15)$$

in which  $R_{\text{td}}$  is the radius at which tidal disruption occurs,  $m$  and  $R_*$  are the mass and radius of the star, respectively, and  $M$  is the mass of the BH. The gravitational field outside a Kerr BH is not Newtonian, but (15) still provides a reasonable estimate of the tidal disruption radius. Comparing this to the Schwarzschild radius of a  $100M_\odot$  BH,  $R_S = 2GM/c^2 = 300 \text{km}$ , suggests that, even when relativistic effects and BH spin are included, tidal disruption could only occur very close to the central BH. Earlier in this section we showed that the orbits of IMRI objects are effectively circular by the time the CO gets close to the IMBH. The tidal effects for stars on circular orbits are most extreme for prograde equatorial orbits, since these come closest to the central body. Thus, we use results for prograde, equatorial circular orbits for a more accurate calculation of tidal disruption.

Vallisneri (2000) analyzed NS disruption using the correct tidal field for objects in prograde, circular, equatorial orbits around a Kerr BH and found that the GW frequency at which tidal disruption occurred,  $f_{\text{td}}$ , satisfied the relationship

$$R_* = \begin{cases} 3.25 \text{km} (m/1.4M_\odot)^{\frac{1}{3}} (M/50M_\odot)^{\frac{2}{3}} (GMf_{\text{td}}/c^3)^{-0.71} & GMf_{\text{td}}/c^3 \leq 0.045 \\ 1.55 \text{km} (m/1.4M_\odot)^{\frac{1}{3}} (M/50M_\odot)^{\frac{2}{3}} (GMf_{\text{td}}/c^3)^{-0.95} & GMf_{\text{td}}/c^3 \geq 0.045 \end{cases} \quad (16)$$

An inspiraling object plunges into the BH when it reaches the innermost stable prograde circular orbit (ISCO). This has radius (Bardeen, Press, & Teukolsky 1972)

$$\begin{aligned} \frac{c^2 R_{\text{isco}}}{GM} &= 3 + \sqrt{3\chi^2 + Z^2} - \sqrt{(3-Z)(3+Z+2\sqrt{3\chi^2+Z^2})}, \\ \text{where } Z &= 1 + \left[ (1+\chi)^{\frac{1}{3}} + (1-\chi)^{\frac{1}{3}} \right] (1-\chi^2)^{\frac{1}{3}}, \end{aligned} \quad (17)$$

where  $\chi = S_1/M^2$  is the dimensionless spin parameter of the BH.

The condition that the star is not disrupted before plunge sets a maximum radius for the NS. If we require the tidal disruption frequency to be greater than the frequency of a prograde circular orbit at the ISCO,  $GMf_{\text{isco}}/c^3 = \{\pi[\chi + (c^2 R_{\text{isco}}/GM)^{3/2}]\}^{-1}$  (Bardeen, Press, & Teukolsky

1972), then Eqs. (16)–(17) imply that the NS escapes disruption provided that

$$R_* < \begin{cases} 7.33\text{km} (m/1.4M_\odot)^{\frac{1}{3}} (M/50M_\odot)^{\frac{2}{3}} \left\{ \chi + [c^2 R_{\text{isco}}/(GM)]^{\frac{3}{2}} \right\}^{0.71} & \chi \leq 0.6894 \\ 4.59\text{km} (m/1.4M_\odot)^{\frac{1}{3}} (M/50M_\odot)^{\frac{2}{3}} \left\{ \chi + [c^2 R_{\text{isco}}/(GM)]^{\frac{3}{2}} \right\}^{0.95} & \chi \geq 0.6894 \end{cases} \quad (18)$$

Reasonable NS models have a maximum radius of  $\sim 16$  km or less, so this criterion will be satisfied for a  $50M_\odot$  IMBH if the spin  $\chi < 0.95$ . For a  $100M_\odot$  IMBH, the condition is satisfied for all spins up to 0.998. As discussed later, we expect IMBHs that grow through minor mergers to have only moderate spin  $\chi \lesssim 0.3$ , so tidal disruption should not occur for such IMBHs.

Although the NS cannot be directly tidally disrupted, tidal oscillations will be excited every time the star passes through periapsis. If sufficient energy is deposited into such tides, the star could eventually be disrupted through this tidal heating (Freitag 2003). To assess whether this effect could be important, we consider the orbital energy lost to leave the star on an orbit with periapsis  $r_p$  and eccentricity  $e$  divided by the binding energy of the star,  $E_{\text{orb}}/E_{\text{bind}}$ . If the inspiral was entirely driven by tidal dissipation, and the tidal energy was not efficiently radiated, this would be the ratio of the energy in tidal oscillations to the stellar binding energy. Under these assumptions, if this ratio was of the order of 1 or more, then tidal heating could disrupt the star. In practice, however, most of the orbital energy is lost to gravitational radiation, since, as we see below, tidal oscillations can only be excited during the late stages of inspiral. Thus, most of the energy does not go into tidal heating, and therefore this ratio would have to be significantly greater than 1 for tidal disruption to occur.

Assuming a Keplerian orbit, this ratio is equal to (Freitag 2003)

$$\frac{E_{\text{orb}}}{E_{\text{bind}}} = 4.8(1 - e) \frac{GM}{c^2 r_p} \left( \frac{R_*}{10\text{km}} \right) \left( \frac{m}{1.4M_\odot} \right)^{-1}, \quad (19)$$

where we have assumed that the star has zero kinetic energy at infinity. (Assuming that the stellar velocity is  $10 \text{ km s}^{-1}$  at infinity changes this result by only  $2.3 \times 10^{-9}$  for a  $1.4M_\odot$  NS of radius 10km.) For an inspiral into a Schwarzschild BH, plunge occurs when  $c^2 r_p(1 + e) = 2(3 + e)GM$ ; therefore for any eccentricity we have  $(1 - e)GM/(c^2 r_p) < 1/6$  at plunge. This means that the energy ratio defined in (19) can only be greater than 1 for  $R_* > 12.5$  km. Tidal disruption due to heating is very unlikely to occur. This conclusion also applies to BHs of moderate spin. For an orbit that is circular at plunge into a BH with spin  $\chi = 0.35$ , the ratio  $E_{\text{orb}}/E_{\text{bind}}$  is approximately equal to 1 at ISCO for  $R_* = 10\text{km}$ .

If systems existed in which an NS was on a prograde inspiral orbit into a rapidly spinning BH, the periapsis at plunge would be much closer to the central body and the energy ratio

would exceed unity at plunge. However, the energy ratio would still be small. The radius of the ISCO for a BH of spin  $\chi = 0.9$  is at  $c^2 r_p = 2.32GM$ , at which radius  $E_{\text{orb}}/E_{\text{bind}} \sim 2$  for  $R_* = 10\text{km}$ . The disruption criterion that  $E_{\text{orb}}/E_{\text{bind}} \sim 1$  assumes that the orbital energy is dissipated entirely by tidal interactions. In practice, the inspiral will mainly be driven by GW emission, since most of the orbital energy is lost in the regime where GW emissions are quite significant. Tidal dissipation would have to occur on a very short timescale to dominate over gravitational radiation reaction effects, and this will not happen in practice. We can thus conclude that disruption of the NS due to tidal heating will not occur. This is in contrast to main-sequence stars that, being less compact, will be disrupted before reaching the ISCO (Freitag 2003). We note that this conclusion does not change when the relativistic orbital energy is used in place of the Keplerian expression.

### 2.5.2. Tidal Capture

Although tidal interactions should not shorten the inspiral by causing disruption of the NS, if orbital energy and angular momentum of the binary are lost into normal modes of the star, the inspiral trajectory will be modified. In principle, this could modify the capture rate and the typical eccentricities expected at plunge. Significant oscillations are only likely to be excited by tidal interactions if the orbital frequency is comparable to the frequency of normal modes in the NS. We can estimate the latter from the frequency associated with the free-fall time in the NS:

$$\omega_{\text{osc}} \approx \frac{\sqrt{2}}{\pi} \sqrt{\frac{Gm}{R_*^3}} = 5.9\text{kHz} \left( \frac{m}{1.4M_\odot} \right)^{\frac{1}{2}} \left( \frac{R_*}{10\text{km}} \right)^{-\frac{3}{2}}. \quad (20)$$

This is just an approximation, but it gives the correct order of magnitude for the normal mode frequency. Press & Teukolsky (1977) computed normal modes using a polytropic stellar model with index  $n = 3$ . They found an  $f$ -mode frequency that agrees with Eq. (20), but with a prefactor of 6.2 kHz instead of 5.9 kHz.

Other stellar modes, in particular  $g$ -modes, can have significantly lower frequency and thus will be excited earlier in the inspiral. Press and Teukolsky tabulate frequencies for  $g$ -modes up to  $g_{14}$ , which has a frequency a factor of 0.15 smaller than the  $f$ -mode. An  $n = 3$  polytrope is not a good model for an NS, but it still provides a reasonable estimate of the frequency range for thermal  $g$ -modes. NSs also support crustal  $g$ -modes that arise from chemical stratification and core  $g$ -modes that arise from stratification in the number densities of charged particles. Finn (1987) computed frequencies of crustal  $g$ -modes in zero-temperature NSs, using a range of stellar models. He found that the longest period modes had periods of  $\sim 20\text{ms}$ . Reisenegger & Goldreich (1992) computed the frequencies of core

$g$ -modes, and found that these have similar frequencies to the crustal modes. Taking  $\sim 50$ ms as a reasonable maximum for the  $g$ -mode period gives a frequency of 20Hz.

Inertial ( $r$ -)modes in rotating NSs typically have frequencies of the order of the spin frequency of the NS ( $f \sim 10 - 100$ Hz). Ho & Lai (1999) examined the excitement of  $r$ -modes by Newtonian tidal driving and found that this was fairly weak. However, Flanagan & Racine (2007) computed the effect of post-Newtonian gravitomagnetic driving and found that this was significantly greater. For rapidly rotating NSs, the inertial-frame frequency can be much smaller than the corotating-frame frequency, which allows  $f$ - and  $p$ -modes to be excited (Ho & Lai 1999). This requires very rapid NS rotation,  $f_{\text{rot}} \sim 500$ Hz. Ho & Lai (1999) examined such modes in the context of comparable mass binaries but concluded that such NS spins were unlikely to be found in binary systems. In the IMRI case, where a free NS is captured, the NS spin could be much higher in principle, making these modes potentially interesting. Ho & Lai (1999) and Flanagan & Racine (2007) considered only modes in the LIGO frequency range,  $10\text{Hz} < f < 1000\text{Hz}$ , but the mode spectrum extends to lower frequencies. However, the frequency at which each resonance occurs is a single-valued function of the spin of the NS.

We compare these frequencies to the orbital frequency of a prograde circular orbit at radius  $r$ :

$$\omega_{orb} = 0.65\text{kHz} \left[ \left( \frac{c^2 r}{GM} \right)^{\frac{3}{2}} + \chi \right]^{-1} \left( \frac{M}{50M_{\odot}} \right)^{-1} \quad (21)$$

Any NS that comes within a distance  $\approx 280GM/c^2$  from an  $M = 100 M_{\odot}$  IMBH will be directly captured as a result of GW emission. The additional energy lost in tidal interactions could increase this capture cross section. However, for  $r = 300GM/c^2$  (cf. § 2.3),  $\omega_{orb} = 0.13$  Hz, which is much less than the frequency of oscillations of the star. The  $g$ -mode frequency is 2 orders of magnitude higher than the orbital frequency at that radius and so it is unlikely to be significantly excited. The  $g$ -mode frequencies become comparable to the orbital frequency for a Schwarzschild BH when  $c^2 r \lesssim 10GM$ . Thus,  $g$ -modes are likely to be excited in the late stages of inspiral, but not earlier. As mentioned above, the spectrum of NS  $r$ -modes and the  $f$ - and  $p$ -mode resonances of rapidly rotating NSs extend to low frequencies (Ho & Lai 1999; Flanagan & Racine 2007). However, the resonant frequencies are determined by the NS spin, so it would require extreme fine tuning for a given NS to be captured at precisely the periapsis that allows excitement of those modes. The capture rate is unlikely to be increased by this mechanism either, although these modes could also be excited later in the inspiral.

Press & Teukolsky (1977) provide an expression for the energy dissipated in tides in an object of mass  $m$  and radius  $R_*$  that passes a point mass of mass  $M$  on a Keplerian orbit

with periapsis  $R_{\min}$ :

$$\Delta E_{\text{tidal}} = \left( \frac{Gm^2}{R_*} \right) \left( \frac{M}{m} \right)^2 \left( \frac{R_*}{R_{\min}} \right)^6 T_2 \left( \sqrt{\frac{m}{M}} \left[ \frac{R_{\min}}{R_*} \right]^{\frac{3}{2}} \right) \quad (22)$$

This expression is integrated over all thermal normal modes, including  $g$ -modes up to  $g_{14}$ . Once again, this result is based on an  $n = 3$  polytropic stellar model, which is not a good model of an NS. However, it should provide an order-of-magnitude estimate for the energy lost in thermal modes. In Eq. (22) we include only the  $l = 2$  modes, since other modes are suppressed by  $(R_*/R_{\min})^2 \ll 1$  relative to these modes. We also take the extreme mass ratio limit  $M \gg m$ . The function  $T_2(\eta)$  behaves as  $T_2(\eta) \sim 0.65\eta^{-2.34}$  at large  $\eta$  (we have derived this “by eye” from Figure 1 in Press & Teukolsky (1977)). We can thus compute the ratio of the energy dissipated in tides to the energy dissipated in GW emission,  $\Delta E_{\text{GW}} = [85\pi m^2 / (12\sqrt{2} Mc^5)] (GM/R_{\min})^{7/2}$ , for an object on a parabolic Keplerian orbit with periapsis  $R_{\min}$ :

$$\frac{\Delta E_{\text{tidal}}}{\Delta E_{\text{GW}}} \approx 0.05 \left( \frac{GM}{c^2 R_{\min}} \right)^{6.01} \left( \frac{R_*}{20\text{km}} \right)^{8.51} \left( \frac{M}{50M_{\odot}} \right)^{-5.34} \left( \frac{m}{1.4M_{\odot}} \right)^{-3.17} \quad (23)$$

It is clear that, under these model assumptions, the tidal perturbation to the orbit at capture is always much weaker than the perturbation induced by GW emission. For comparison, since  $\Delta E_{\text{GW}} \propto r_p^{-7/2}$ , a 10% increase in the energy lost in a single pass by the central BH increases the minimum periapsis required for direct capture by only a factor of  $1.1^{2/7} \approx 1.03$  or  $\sim 3\%$ .

The above arguments indicate that the excitement of NS modes will neither increase the capture rate nor lead to NS disruption during an IMRI. However, orbital energy lost into oscillations could modify the inspiral trajectory by either causing a cumulative phase shift in the emitted GWs or changing the eccentricity of the orbit in the LIGO band. Flanagan & Racine (2007) calculated the phase difference in the GWs that arises from the excitement of  $r$ -modes, finding  $\Delta\Phi \sim 3.4R_{10}^4 f_{s100}^{2/3} M_{1.4}^{-1} m_{1.4}^{-2} (M_{1.4} + m_{1.4})^{-1/3}$ , where  $R_{10}$  is the NS radius in units of 10km,  $M_{1.4}/m_{1.4}$  are the masses of the primary/secondary in units of  $1.4M_{\odot}$ , and  $f_{s100}$  is the spin frequency (or  $r$ -mode frequency) in units of 100 Hz. For an IMRI with  $M = 50M_{\odot}$ , this gives  $\Delta\Phi \sim 0.003$  if we set  $R_{10} = f_{s100} = m_{1.4} = 1$ . Typically we require a phase shift of  $\Delta\Phi \sim 1$  for an effect to be observable, so the excitement of  $r$ -modes will not leave an imprint on the inspiral. The phase shift induced by the resonant excitement of  $f$ - and  $p$ -modes in rapidly rotating NSs can be significantly higher. Ho & Lai (1999) quote  $\Delta\Phi \sim 234m_{1.4}^{-4.5} R_{10}^{3.5} m_{1.4}^2 / (M_{1.4}(m_{1.4} + M_{1.4})) f_{gw100}^{-1}$  for the most extreme case of the (22, 2)  $f$ -mode resonance (with the same notation as before but now denoting the GW frequency in units of 100 Hz by  $f_{gw100}$ ). For an  $M = 50M_{\odot}$  IMRI, this gives  $\Delta\Phi \sim 0.2f_{gw100}^{-1}$ . This could be a measurable shift if the resonance is excited near 10 Hz. However, the phase shift is only

this large for IMBHs at the low-mass end of the IMRI range, and provided that the NS spin is tuned to ensure that the resonance is excited near 10 Hz. More work will be needed to quantify how large a phase shift would be measurable with Advanced LIGO, accounting for correlations between the waveform parameters.

We can estimate qualitatively what effect tidal dissipation would have on the orbital eccentricity and periapsis. The phase-space trajectory that an inspiral follows is determined entirely by the ratio  $dE/dL_z$ . Assuming a Keplerian orbit, we have

$$\frac{dr_p}{de} = \frac{r_p \left( 2 \sqrt{(1+e)GM} - r_p^{\frac{3}{2}} dE/dL_z \right)}{(1+e) r_p^{\frac{3}{2}} dE/dL_z - 2(1-e) \sqrt{(1+e)GM}}. \quad (24)$$

We now suppose that the inspiral was driven entirely by tidal dissipation. Typically the dominant excited mode would be an  $m = 2$  mode, for which  $\Delta L_z = 2\Delta E/\omega_{00}$ , where  $\omega_{00}$  is the frequency of the mode (this assumes that the stellar oscillations can be modeled as a linear Lagrangian system; Friedman & Schutz 1978). We write

$$\omega_{00} = \sqrt{\frac{GM}{r_c^3}}, \quad (25)$$

where  $r_c$  is the radius of the circular (Keplerian) orbit that would have the same frequency as the  $m = 2$  mode. With this substitution, equation (24) defines the evolution of  $r_p/r_c$  over the inspiral. Equations (20) and (21) indicate that the capture periapsis,  $r_p^0$ , will typically be much greater than  $r_c$ . Solutions with  $r_p^0 > 2^{5/3}r_c$  are all qualitatively the same, and we show a typical example in Figure 2, for capture periapsis of  $1000 r_c$  and a capture eccentricity of 1. For a  $100M_\odot$  IMBH, taking  $\omega_{00} = 6$  kHz yields  $c^2 r_c \approx 0.5GM$ , so this figure represents a capture at  $r_p \approx 500 GM/c^2$ , the upper end of the allowed direct capture range for an  $m = 10 M_\odot$  BH. The figure shows the inspiral in eccentricity-periapsis space. Under this simple model of tidal interactions, the periapsis increases while the eccentricity decreases. In practice, the inspiral will be driven by a combination of GW emission and any tidal dissipation that occurs. These results suggest that tidal effects would tend to make the eccentricities at plunge smaller than they would be for inspirals driven by radiation reaction alone.

Equations (20)–(23) indicate that normal modes are unlikely to be excited during an inspiral into an IMBH, although high-order  $g$ -modes,  $r$ -modes, and  $f$ -modes in rapidly rotating NSs might be excited during the very late stages of inspiral. Thus, we can safely ignore the effect of tides on the capture rates. Tidal effects could modify the inspiral, although the above calculation indicates that this should not modify our conclusions about the typical eccentricities at plunge. The excitement of  $f$ -modes might leave a measurable imprint on

the GW signal. However, the induced phase shift is only marginally detectable, and this mechanism requires the NS to be rapidly rotating.

### 3. Event Rates

In this section we estimate the rate of IMRIs in globular clusters detectable by Advanced LIGO. To do this, we must consider three elements: (1) the distance sensitivity of the detectors to GWs from IMRIs (and hence the volume of the universe the detectors can see), (2) the number density of globular clusters, and (3) the rate of IMRIs per globular cluster.

#### 3.1. Advanced LIGO IMRI Sensitivity

For GW sources with known waveforms (or at least waveforms well approximated by analytic or numerical techniques), matched filtering is used to search for signals in GW detector data (Wainstein & Zubakov 1962; Allen et al. 2005). The S/N  $\rho$  of a template  $h(t)$  in data  $s(t)$  collected by a detector that has one-sided noise power spectral density  $S_n(|f|)$  is given by

$$\rho = \frac{4}{\sigma} \int_0^\infty \frac{|\tilde{s}(f)\tilde{h}^*(f)|}{S_n(|f|)} df, \quad (26)$$

where  $\tilde{s}(f)$  is the Fourier transform of the signal  $s(t)$ ,  $\tilde{h}(f)$  is the Fourier transform of the inspiral template  $h(t)$ , the asterisk denotes complex conjugation, and  $\sigma$  is defined by

$$\sigma^2 = 4 \int_0^\infty \frac{|\tilde{h}(f)|^2}{S_n(|f|)} df. \quad (27)$$

This definition of S/N follows the normalization of Cutler & Flanagan (1994) and Allen et al. (2005). We place the template  $h(t)$  at a canonical source distance of 1 Mpc and choose the optimal orientation of the detector to maximize the S/N, and so the maximum distance to which a single detector matched filter search is sensitive at a given S/N  $\rho$  is given by  $D = \sigma/\rho$  Mpc. (This is the same quantity as the “inspiral horizon distance” used by the LIGO and Virgo Collaborations Abbott et al. (2008).)

To compute the sensitivity of a single Advanced LIGO detector to IMRIs, we need to compute the quantity  $\sigma^2$  defined in Eq. (27) using a particular waveform model. We have done this with waveforms based on BH perturbation theory (Finn & Thorne 2000), which are valid in the limit  $m/M \ll 1$ . The waveforms, which include non-quadrupolar harmonics of the orbital frequency in addition to the dominant quadrupolar harmonic, are

described in Appendix A, where we also discuss the relative S/N contributed by the four lowest harmonics. The noise power spectral density  $S_n(|f|)$  was taken from Fritschel (2003). GW detectors have an orientation-dependent response. The relation between the *range*  $R$  (defined as the radius of a sphere whose volume is equal to the volume of the universe in which inspiral sources could be detected with an S/N threshold of  $\rho$ ) and maximum distance  $D$  at a fixed S/N is given by  $R = D/2.26$  (Finn & Chernoff 1993).

We assume a value of  $\rho = 8$  for the threshold S/N required for a detection, since this is the value typically used to compute Initial LIGO detection ranges for comparable-mass black hole binaries (Abbott et al. 2008). This is a reasonable approximation, as a binary black hole inspiral with a total mass of  $6 M_\odot$  has approximately 500 GW cycles between the 40 Hz low-frequency cutoff of Initial LIGO and coalescence — roughly the same number of GW cycles that an IMRI signal in Advanced LIGO will have between the Advanced LIGO low-frequency cutoff of 10 Hz and coalescence. The threshold will be computed more accurately when an IMRI search is implemented and the amount of non-stationarity of the Advanced LIGO data is known. If the  $\rho = 8$  threshold cannot be achieved in practice (or if it can be improved), then the detection rates derived below can be scaled appropriately.

Advanced LIGO will consist of a network of three 4-km detectors. Demanding that GWs are found coincident in all three detectors increases the network range by a factor of  $\sqrt{3}$  relative to the range of a single detector at a given S/N (due to the lower false alarm rate of the network). Fig. 3 shows the range  $R$  of a network of three Advanced LIGO detectors for circular-equatorial-orbit IMRIs of  $m = 1.4M_\odot$  objects into a Kerr IMBH of mass  $M$ , assuming that the network S/N required for a confident detection was  $\rho = 8$ . This is equivalent to the range of a single detector with S/N of  $\rho = 8/\sqrt{3}$ . The  $\chi = 0$  (non-spinning IMBH) line in Fig. 3 is well-approximated by a quadratic fit:

$$R \approx \sqrt{m/M_\odot} \times \left[ 800 - 540 \left( \frac{M}{100 M_\odot} \right) + 107 \left( \frac{M}{100 M_\odot} \right)^2 \right] \text{ Mpc.} \quad (28)$$

The scaling of the range in Eq. (28) as  $\sqrt{m}$  does not follow from the fit, but rather from the following reasoning. The amplitude of GWs from IMRIs will scale linearly with the mass of the smaller object  $m$ , but the number of cycles in the LIGO band will also drop by roughly a factor of  $m$ . Hence, the total S/N will grow as  $\sqrt{m}$ , so inspirals of more massive COs will be seen a factor of  $\sqrt{m}$  farther away.

The combination of the spin of the central object and the inclination of the orbital plane of the inspiraling particle will have a significant effect on the signal from an IMRI. The frequency of the ISCO is much higher for prograde inspirals into rapidly spinning BHs than for inspirals into non-spinning holes; the S/N can be strongly enhanced for such orbits.

Conversely, retrograde inspirals will have lower S/R. Averaging over random inclination angles, Mandel (2007) computed the ratio between (1) the detection range for Advanced LIGO in a universe uniformly populated by IMBHs of a given mass and spin and (2) the detection range in a universe with an equal density of Schwarzschild IMBHs with the same mass. He found that the detection range can be enhanced by a factor of 1.7 (3.8) for maximally spinning Kerr BHs with  $M = 100M_\odot$  ( $M = 200M_\odot$ ); the increase in the volume of observable space and, hence, the event rates, is the cube of these numbers.

If IMBHs grow mainly by random mergers, they will not be rapidly spinning as the contributions of subsequent mergers to the hole’s spin largely cancel out. The angular momentum imparted to the IMBH by a CO is  $L_{\text{obj}} \propto mM$ , since the radius at ISCO is  $r_{\text{ISCO}} \propto M$ . This causes the dimensionless spin parameter of the hole  $\chi = S_1/M^2$  to change by  $\sim L_{\text{obj}}/M^2 \propto m/M$ . After  $\sim M/m$  such mergers, necessary for the hole to grow to mass  $M$ , the typical spin of the hole will be  $\chi \sim \sqrt{m/M}$ . More precise calculations (Hughes & Blandford 2003; Miller 2002; Mandel 2007) show that the spin of IMBHs involved in LIGO IMRIs will rarely exceed  $\chi = 0.3$  for IMBHs that gained a significant fraction of their mass via minor mergers. For small values of  $\chi$ , Eq. (24) of Mandel (2007) yields a correction to the range presented in Eq. (28) due to the inclusion of the IMBH spin; the detection range in Mpc as a function of  $M$ ,  $m$ , and  $\chi$  is

$$\frac{R}{\text{Mpc}} \approx \left[ 1 + 0.6 \chi^2 \left( \frac{M}{100 M_\odot} \right) \right] \sqrt{\frac{m}{M_\odot}} \left[ 800 - 540 \left( \frac{M}{100 M_\odot} \right) + 107 \left( \frac{M}{100 M_\odot} \right)^2 \right]. \quad (29)$$

This range estimate does not include the cosmological redshift. The redshift due to the expansion of the universe decreases the frequency of the GWs. For  $M \sim 100 M_\odot$  IMRIs, the redshifted GWs will lie in a less sensitive part of the LIGO noise curve, thereby reducing the range. For IMRIs detectable with Advanced LIGO, redshifts are typically  $\lesssim 0.2$ ; for example, the inspiral of a  $1.4M_\odot$  NS into a non-spinning  $100M_\odot$  IMBH is visible to a redshift of 0.09. We estimate that for typical sources, properly including the redshift reduces the Advanced LIGO event rate by  $\sim 10\%$ .

Advanced LIGO will have several parameters that may be tuned during the operation of the detector to optimize the noise power spectral density (PSD) in order to search for specific sources. These tunable parameters include the laser power and the detuning phase of the signal recycling mirror. If a noise PSD optimized for detections of CO–IMBH binaries is used instead of the default PSD assumed in Fig. 3, the range for such sources is increased by a factor of  $\sim 1.5$ , corresponding to an event rate increase by a factor of  $\sim 3.5$ .

### 3.2. Number Density of Globulars with a Suitable IMBH

The second element in the rate calculation is the number density of globular clusters that have an IMBH in the relevant mass range. This is highly uncertain. To contribute significantly, a cluster must have had a sufficiently small initial relaxation time to allow the formation of an IMBH through some mild runaway process when the cluster was young, yet not have formed an IMBH with  $M > 350 M_{\odot}$  (since this would put IMRIs beyond the Advanced LIGO frequency range). Recent theoretical arguments by Trenti and colleagues (Heggie, Trenti, & Hut 2006; Trenti et al. 2007; Trenti, Heggie, & Hut 2007; Trenti 2006) suggest that dynamically old globulars with large core to half-mass radius ratios have been heated by a  $\sim 1000 M_{\odot}$  IMBH, so these clusters would not contribute to the Advanced LIGO IMRI rate. Note, however, that Hurley (2007) has shown that current observations of the core-to-half-light ratios in globulars do not require  $1000 M_{\odot}$  BHs in most clusters. Core-collapsed globular clusters, which constitute  $\sim 20\%$  of all globular clusters (Phinney 1991), may contain IMBHs of the right mass. We will parametrize the unknown fraction of relevant globular clusters by some fraction  $f$ . Globular clusters have a space density of  $8.4 h^3 \text{ Mpc}^{-3}$  (Portegies Zwart & McMillan 2000), which for  $h = 0.7$  yields  $2.9 \text{ Mpc}^{-3}$ . Therefore, we will use the number density  $\sim 0.3 (f/0.1) \text{ Mpc}^{-3}$ . This factor  $f$  depends on both the number of clusters with an IMRI in the right mass range and the number of clusters that have been in a state of core-collapse long enough for the binary hardening mechanism to occur. These factors are degenerate, however, since clusters with heavier IMBHs will not be in a state of core collapse, as described above. The fraction  $f$  also depends on what proportion of the objects merging with the IMBH are COs as opposed to main-sequence stars. Our Monte Carlo simulations, which were discussed earlier, indicate that this proportion is close to 1.

The fraction  $f$  of globular clusters containing IMBHs may be further lowered by ejections of IMBHs from their clusters by recoil kicks imparted to the IMBHs by dynamical processes and by gravitational radiation emission. If the kick exceeds  $\approx 50 \text{ km s}^{-1}$ , which is the escape velocity from a massive globular cluster, the IMBH will escape from the cluster, thereby becoming unavailable for future events. Kicks can arise from the process of hardening via three-body encounters (Kulkarni, Hut, & McMillan 1993; Sigurdsson & Hernquist 1993; Gültekin, Miller, & Hamilton 2004, 2006). Gültekin, Miller and Hamilton (2006) show (cf. their Fig. 12) that when the seed mass is  $100 M_{\odot}$ , only about 50% of all BHs grow to  $300 M_{\odot}$  without being ejected, and this fraction drops to 10% for a seed mass of  $50 M_{\odot}$ .

Kicks also arise from GW emission. During the last stages of the merger of unequal mass BHs, a net flux of angular momentum will be carried away by the GWs, imparting a kick to the resulting BH (Peres 1962; Bekenstein 1973; Fitchett 1983; Fitchett & Detweiler 1984; Redmount & Rees 1989; Wiseman 1992; Favata, Hughes, & Holz 2004; Blanchet, Qusailah, & Will

2005; Damour & Gopakumar 2006; Herrmann et al. 2007a; Baker et al. 2006; Gonzalez et al. 2007a; Sopuerta, Yunes, & Laguna 2007). The most recent results on merger velocity kicks, based on numerical relativity, show that the kick velocity for a non-spinning central object depends on the symmetric mass ratio  $\eta = mM/(m + M)^2$  as  $V_{\text{kick}} \approx 12000\eta^2\sqrt{1 - 4\eta}(1 - 0.93\eta)$  km s<sup>-1</sup> (Gonzalez et al. 2007a). The requirement  $V_{\text{kick}} < 50$  km s<sup>-1</sup> places an upper limit on  $m$  of  $q = m/M \lesssim 0.08$ .

If the IMBH is rapidly spinning, recent numerical relativity results suggest that the kick can be a lot higher (Baker et al. 2007; Campanelli et al. 2007a,b; Gonzalez et al. 2007b; Herrmann et al. 2007b; Koppitz et al. 2007). Baker et al. (2007) and Campanelli et al. (2007a) provide a fit to numerical relativity results that gives the kick as a function of the various orbital parameters. This formula indicates that if the IMBH has moderate spin  $\chi \lesssim 0.5$  and the secondary is non-spinning, then we require  $q \lesssim 0.05$  to ensure that the IMBH has a high probability of remaining in the globular cluster today after undergoing multiple mergers. This constraint can be relaxed to  $q \lesssim 0.067$  if  $\chi \lesssim 0.3$ . If the objects merging with the IMBH are BHs with a mass of  $10M_{\odot}$ , this constrains the initial IMBH mass to be  $M \gtrsim 150M_{\odot}$ . If the merging objects are  $1.4M_{\odot}$  NSs, even IMBHs with a seed mass of  $50M_{\odot}$  are safe from ejection.

As argued earlier, mergers with BHs are likely to be important early in the IMBH evolution, when its mass is smaller, with NS mergers becoming dominant later. This could mean that a significant number of IMBHs were ejected from globular clusters early in their evolution. However, without firm knowledge of the initial seed masses of IMBHs or the relative number of mergers with BHs and NSs that each IMBH undergoes, it is impossible to draw definitive conclusions. We normalize  $f$  to 10% in the rate calculations that follow, but we emphasize that this quantity is highly uncertain at present.

### 3.3. IMRI Rate per Globular Cluster and Event Rate

The final contribution to the rate estimate is the merger rate per globular cluster. Existing numerical simulations of globular clusters suggest that mergers in the subcluster of  $\sim 10M_{\odot}$  BHs at the center of the globular cluster can lead to the creation of IMBHs with masses up to  $\sim 350M_{\odot}$  in  $\sim 10^{10}$  yr (O’Leary et al. 2006). However, the results of such simulations are very sensitive to the choice of cluster models and to assumptions about kick velocities, the interaction between the BH subcluster and the rest of the cluster, etc. Therefore, we present two methods for computing the rate per globular: (1) an upper limit independent of cluster model and (2) an estimate based on a more realistic model for cluster dynamics.

We estimate a theoretical upper limit on the IMRI event rate in a globular cluster using the following method, originally suggested by Phinney (2005). We assume that each globular cluster has a BH that grows from  $M \sim 50M_\odot$  to  $M \sim 350M_\odot$  by capturing a sequence of COs of identical mass  $m$  over the age of the cluster. Then  $300M_\odot/m$  captures will happen in each globular cluster in  $\sim 10^{10}$  yr. This leads to a rate of  $(300 M_\odot)/m \times (10^{10} \text{ yr})^{-1}$  per cluster.

Although this rate is plausible, it may be a significant over-estimate for several reasons. First, it assumes that all the mass that the IMBH acquires in growing from  $M \sim 50M_\odot$  to  $M \sim 350M_\odot$  comes from mergers with COs. In practice, the IMBH will also acquire mass via gas accretion, and by captures of main-sequence stars and white dwarfs, which will be tidally disrupted before becoming significant GW sources but will still add mass to the IMBH. Second, this estimate does not include the likelihood that the merger product will be kicked out of the cluster through recoil, as discussed in the previous section. Third, this estimate assumes that the rate at which the IMBH grows via IMRIs from  $50 M_\odot$  to  $350 M_\odot$  is constant in time. However, Advanced LIGO can only detect mergers that occurred at distances  $\lesssim 1$  Gpc, i.e., relatively recently, so the relevant rate is the rate late in the history of the globular cluster, which is likely to be much lower. For example, O’Leary et al. (2006) found in their numerical simulations that the rate dropped from  $\sim 10^{-7}$  to  $\sim 3 \times 10^{-10} \text{ yr}^{-1}$  after  $10^{10}$  yr for some plausible cluster models.

For the theoretical upper limit, the total rate is given by  $\alpha \overline{V(M, m, \chi)}$ , where  $\alpha \sim 0.3 (f/0.1) \text{ Mpc}^{-3} (300 M_\odot)/m (10^{10} \text{ yr})^{-1}$  is the IMRI rate in the universe,  $V(M, m, \chi) = (4/3)\pi R^3$  is the volume in which Advanced LIGO can see an event, and on overbar,  $\overline{V}$ , denotes the average over mass  $M$  in the range between  $50M_\odot$  and  $350M_\odot$ . If we take  $f = 0.1$ ,  $\chi = 0.2$  as the typical IMBH spin, and all inspiraling objects are  $1.4M_\odot$  NSs, the event rate is  $\approx 3 \text{ yr}^{-1}$ ; if  $f = 0.1$ ,  $\chi = 0.2$ , and inspiraling objects are  $10M_\odot$  BHs, the event rate is  $\approx 10 \text{ yr}^{-1}$ . These values are based on the range fit in Eq. (29), so they assume that orbital frequency harmonics through  $m = 4$  are included in the data analysis, but cosmological redshift and Advanced LIGO optimization are not included. When all of these considerations are taken into account, a theoretical upper-limit estimate suggests that Advanced LIGO may detect up to 30 IMRIs per year. A similar estimate for Initial LIGO shows that because of lower overall sensitivity and a higher low-frequency cutoff (40 Hz for Initial LIGO vs. 10 Hz for Advanced LIGO), the upper limit on the Initial LIGO IMRI rate is only about 1/1000 events  $\text{yr}^{-1}$ .

A more realistic estimate is based on the assumption that the hardening of a CO–IMBH binary via three-body interactions represents the primary capture mechanism leading to IMRIs. The rate for IMRIs created by this scenario is  $\approx 3 \times 10^{-9} \text{ yr}^{-1}$  per globular

cluster for NS–IMBH IMRIs and  $\approx 5 \times 10^{-9} \text{ yr}^{-1}$  for BH–IMBH IMRIs [see § 2.1]. Hence, the NS–IMBH IMRI rate in the local universe is  $\alpha \approx 10^{-9} (f/0.1) \text{ Mpc}^{-3} \text{ yr}^{-1}$ , while the BH–IMBH IMRI rate is  $\alpha \approx 1.5 \times 10^{-9} (f/0.1) \text{ Mpc}^{-3} \text{ yr}^{-1}$ . If we assume that all IMBHs have a mass  $\sim 100M_{\odot}$  and  $f = 0.1$ , this yields an Advanced LIGO rate of one IMRI per 3 years if the typical CO is an NS or 10 IMRIs per year if the typical CO is an  $m = 10 M_{\odot}$  BH. If the interferometer is optimized for the detection of IMRIs, the NS–IMBH and BH–IMBH rates are increased to 1 and 30 events  $\text{yr}^{-1}$ , respectively.

In addition to detections of inspirals, Advanced LIGO could also detect the ringdown of an IMBH following a merger. This possibility is discussed in Appendix B.

#### 4. Effect of Eccentricity on Matched Filter Searches

As discussed in § 3.1, matched filtering is used to search for GWs with known waveforms in detector noise. In order to be an optimal search technique, the matched filter requires accurate templates that correctly model the signals being sought (Wainstein & Zubakov 1962). Since source parameters (e.g., the masses and the IMBH spin) can vary, the matched filter is constructed for a “bank” of templates: a set of waveform models that depend on the parameters that characterize the source. The accuracy of a template bank is characterized by the fitting factor (FF) (Apostolatos 1996), which measures the overlap between the GW signal and the nearest template. A fitting factor close to unity indicates that the templates are accurate for detection of the desired signals. A fitting factor less than unity will mean that we are unable to detect a fraction  $(1 - \text{FF}^3)$  of the theoretically detectable events. (The quantity  $1 - \text{FF}$  is often referred to as the mismatch.) To search for signals, template banks are constructed so that the mismatch between any desired signal and the nearest template does not cause an unacceptable loss in S/N (typically  $\text{FF} \approx 0.97$  for LIGO).

In this section we examine the effect of eccentricity on searching for IMRI signals in Advanced LIGO detectors. The effect of eccentricity on the fitting factor was previously examined by Martel & Poisson (1999), and it was found that the fitting factor between a circular and eccentric waveform template was high provided that  $e \lesssim 0.2$ . However, their results do not apply directly to IMRIs since they computed fitting factors only for binaries with mass ratios close to 1, and used the first-generation LIGO noise curve.

We consider a matched-filter search for IMRIs and determine the loss in S/N (and hence range) if eccentricity is not included in the template bank; i.e., circular templates are used to search for potentially eccentric waveforms. We compute the fitting factor as follows. The template  $h(t)$  appearing in the expression for the matched filter S/N  $\rho$  [Eq. (26)] depends

on a number of parameters characterizing the source, such as the masses of the binary and the time of arrival of the signal. We denote these parameters  $\vec{\lambda}$  and define the ambiguity function  $\mathcal{A}(\vec{\lambda})$  by

$$\mathcal{A}(\vec{\lambda}) = \frac{\langle s|h(\vec{\lambda}) \rangle}{\sqrt{\langle s|s \rangle \langle h(\vec{\lambda})|h(\vec{\lambda}) \rangle}}, \quad (30)$$

where  $\langle a|b \rangle$  is the matched filter inner product given by

$$\langle a|b \rangle = 4 \int_0^\infty \frac{\tilde{a}(f)\tilde{b}^*(f)}{S_n(|f|)} df. \quad (31)$$

We separate the parameters  $\vec{\lambda}$  into  $\vec{\lambda} = (t_0, \phi_0, \vec{\theta})$ , where  $t_0$  and  $\phi_0$  are the time of arrival and phase of the binary, respectively. In the case of circular equatorial binaries, it is trivial to maximize over the parameters  $t_0$  and  $\phi_0$  analytically (the phase by projecting the signal onto two orthogonal basis vectors and the time by a Fourier transform), and so these are called “extrinsic parameters.” The remaining template parameters  $\vec{\theta}$ , which include the binary masses, eccentricity, and IMBH spin, determine the shape of the waveform and are known as “intrinsic parameters.” For circular inspiral templates, the ambiguity function  $\mathcal{A}$  reduces to the overlap  $\mathcal{O}$ , given by

$$\mathcal{O}(\vec{\theta}) = \max_{t_0, \phi_0} \frac{\langle s|h(\vec{\theta}) \rangle}{\sqrt{\langle s|s \rangle \langle h(\vec{\theta})|h(\vec{\theta}) \rangle}}, \quad (32)$$

The fitting factor is given by the maximum of the overlap function over the remaining parameters

$$\text{FF} = \max_{\vec{\theta}} \mathcal{O}(\vec{\theta}). \quad (33)$$

For the signal  $s(t)$  and template  $h(t)$  we use numerical kludge waveforms. This is a family of waveforms that were constructed as models for extreme mass ratio inspiral systems, in which  $m/M \ll 1$ . The waveform family is constructed by first computing an accurate phase-space trajectory by integrating prescriptions for the evolution of the orbital elements (the orbital energy, angular momentum, and Carter constant, or equivalently the orbital radius, eccentricity, and inclination) (Gair & Glampedakis 2006). The orbit of the small body is then calculated by integration of the Kerr geodesic equations along the sequence of geodesics defined by the phase-space trajectory. Finally, a kludge waveform is generated from the orbit by applying weak-field emission formulae (Babak et al. 2007). This waveform family predicts the inspiral rates for nearly-circular orbits very well (Gair & Glampedakis 2006) and has been shown to be extremely faithful (overlaps in excess of  $\sim 95\%$  over much of the parameter space) to more accurate perturbative waveforms (Babak et al. 2007). Although

the mass ratio of an IMRI system is probably too high to make these waveforms accurate as search templates, they should provide reliable predictions of the fitting factor.

For these calculations we used  $M = 100 M_\odot$  for the IMBH mass,  $m = 1.4 M_\odot$  for the companion mass, and considered two spin values  $\chi = 0$  and  $\chi = 0.2$ . We used the Advanced LIGO power spectral density  $S_n(|f|)$  given by Fritschel (2003). As discussed above, to compute the fitting factor one must maximize over the parameters  $\vec{\theta}$  of the template. However, we find that even without maximizing over the intrinsic parameters, the overlap (and hence the fitting factor) between circular and eccentric templates is greater than 0.99 for eccentricities  $e < 0.01$ , i.e., for more than two-thirds of IMRIs formed by direct capture (the mechanism likely to give the largest eccentricities). Since we expect that most of the IMRI systems will have eccentricities significantly less than  $e = 0.01$  by the time they have entered the Advanced LIGO band, eccentricity will be negligible for data analysis and circular templates may be used to search for these systems.

Fig. 4 shows the overlap between eccentric signals and circular templates for prograde equatorial inspirals and eccentricities greater than 0.01. Analysis of inclined inspirals demonstrates that the overlaps between eccentric signals and circular templates remain greater than 0.99 for eccentricities  $e < 0.01$  and greater than 0.93 for eccentricities  $e < 0.05$ . Although the overlap decreases for eccentricities greater than 0.01, we anticipate higher values of the fitting factor when we maximize over the other intrinsic parameters. An interesting question will be to determine whether eccentricities greater than 0.01 can be measured (and thus be used to investigate the relative prevalence of the various capture mechanisms) or if eccentricity is degenerate with masses and the other intrinsic parameters.

## 5. Summary

In this paper we have discussed a potential source of GWs for ground-based interferometers: the intermediate mass ratio inspiral of a stellar mass CO (an NS or BH) into an IMBH in the center of a globular cluster. For IMBHs with masses in the range  $50 - 350 M_\odot$ , the GWs emitted will be at frequencies in the Advanced LIGO band. We have shown that Advanced LIGO should be able to detect the inspiral of a  $1.4 M_\odot$  NS into an IMBH at distances up to 700 Mpc, depending on the mass and spin of the IMBH. Assuming that all IMBHs were grown by CO–IMBH mergers gives an upper limit on the Advanced LIGO event rate of  $\sim 10 \text{ yr}^{-1}$ . We have shown that if the inspiraling CO is an NS, a more likely estimate of the rate is one event per 3 years, while the rate for BH–IMBH IMRIs could reach the upper limit. If Advanced LIGO is optimized for detections at low frequencies, the event rate estimates would increase by a factor of  $\sim 3.5$ .

We have also discussed four mechanisms by which such IMRI systems could form: (1) binary hardening via three-body interactions, (2) hardening via Kozai resonance, (3) direct capture, and (4) tidal capture of a main-sequence star. In all four cases, we find that the residual eccentricity when the inspiral enters the LIGO sensitivity band will be small. Finally, we have estimated the sensitivity of Advanced LIGO to the eccentricity of IMRI systems. We have found that the eccentricities we expect are negligible for data analysis, and therefore circular-orbit templates may be used to search for IMRI binaries in Advanced LIGO.

IMRIs are a somewhat speculative source of GWs, since evidence for the existence of IMBHs is not yet conclusive. The body of evidence is steadily growing, however. Since little is known about the abundance of IMBHs in the universe, the event rates presented here are naturally somewhat uncertain. However, our results are sufficiently promising to make IMRIs a source worth searching for in Advanced LIGO data. If IMRI events are detected with Advanced LIGO, these will provide irrefutable evidence for the existence of BHs with intermediate mass and will provide information on the mass and spin of IMBHs, plus the eccentricities of the inspiraling objects. This information will be very useful for constraining models of IMBH formation and growth and for exploring stellar dynamics in the centers of globular clusters.

The authors are grateful to Sterl Phinney, Kip Thorne, Yuri Levin, Clovis Hopman, and Teviet Creighton for helpful discussions. I.M. thanks the Brinson Foundation, NASA grant NNG04GK98G, and NSF grants PHY-0601459 and PHY-0653321 for financial support. M.C.M. acknowledges support from the National Science Foundation under grant AST 06-07428. J.G.’s work was supported by St. Catharine’s College, Cambridge. D.B. acknowledges support from the LIGO Laboratory and the National Science Foundation under grant PHY-0601459. LIGO was constructed by the California Institute of Technology and Massachusetts Institute of Technology with funding from the National Science Foundation and operates under cooperative agreement PHY-0107417. This paper has LIGO Document Number LIGO-P070014-00-Z.

## APPENDIX

### A. Waveforms and Signal-to-Noise Ratio Calculation

To compute the range to which a source can be seen, as presented in § 3.1, we must evaluate the S/Ns of typical sources. To do this requires a model of the waveform. In the weak field, waveforms may be well approximated by post-Newtonian results. The leading-

order post-Newtonian result takes the system to be a Keplerian binary and estimates the gravitational radiation from the leading-order quadrupole formula (Peters & Mathews 1963; Peters 1964). This predicts  $\tilde{h}(f) \propto f^{-7/6} \Theta(f - f_{\text{ISCO}})$ , where the step function  $\Theta$  is included to ensure that the radiation cuts off at  $f_{\text{ISCO}}$ , the GW frequency at the innermost stable circular orbit of the binary. The post-Newtonian results are a weak field expansion and are only valid where velocities are much less than the speed of light. As a consequence, the leading-order post-Newtonian waveforms over-predict the S/N of an IMRI source, since they effectively spend too many cycles at each frequency as the ISCO is approached.

An alternative GW model can be obtained from perturbation theory, by expanding in terms of the mass ratio,  $m/M$ , assumed to be small. The IMRI systems considered in this paper lie somewhere between these two extremes — the mass ratio is not quite small enough to use perturbative techniques, but the source spends a long time in the regime where post-Newtonian results are not valid. Waveform models have not yet been developed specifically for IMRI systems. However, by the time Advanced LIGO comes online, it is likely that models will have been constructed by combining post-Newtonian and perturbative techniques. This is discussed in more detail by Amaro-Seoane et al. (2007). If accurate waveforms are not available, we will require sources to have higher S/Ns to be detected, thus reducing the ranges from the values that we quote. However, the loss in S/N from using an inaccurate template is likely to be only a few tens of percent (Amaro-Seoane et al. 2007), which is considerably smaller than the uncertainties in the astrophysical mechanisms that govern the event rates we are computing.

Out of the set of currently available waveform families, we believe that the most accurate S/Ns will come from the perturbative waveforms. Although the perturbative waveform will not be a precise model of the true waveform, the total energy content of the GWs will be roughly correct since the perturbative methods use a reliable model of the spacetime close to the central BH. To generate the range estimates quoted in this paper, we therefore computed the S/N via a perturbative model, as described below.

Finn & Thorne (2000) used perturbation theory to compute the S/N, averaged over sky location and source orientation, contributed by the lowest four harmonics of the orbital frequency for circular, equatorial inspirals into Kerr BHs. Their calculation is accurate in the sense that it is based on perturbation theory, but it relies on three assumptions: (1) the orbit is in the extreme mass ratio limit, i.e.,  $m/M \ll 1$ ; (2) the orbit of the small body is circular; and (3) the orbit of the small body is equatorial. Assumption (2) is valid for our case, and assumption (1) is probably sufficiently accurate (the mass ratio here is intermediate while not extreme). Assumption (3) is not necessarily valid, but we can derive results for both prograde and retrograde equatorial orbits from the Finn & Thorne (2000) waveforms and

then average over possible orbital inclinations of the inspiraling object by assuming that the effect of averaging is the same as it is for the leading-order post-Newtonian model (Mandel 2007).

It is conventional to use  $m$  to denote harmonic number when discussing harmonics of the azimuthal frequency. However, in this paper we use  $k$  to avoid confusion with the mass of the CO. The S/N contributed by the  $k$ th harmonic of the orbital frequency,  $f_k = k\omega_{orb}/(2\pi)$ , and averaged over sky location and source orientation is given by (Finn & Thorne 2000)

$$\rho_k^2 = \int \frac{[h_{c,k}(f_k)]^2}{f_k S_n(f_k)} d \ln f_k, \quad (\text{A1})$$

where  $S_n(f)$  is the one-sided power spectral density of the detector noise and  $h_{c,k}(f_k)$  is the characteristic amplitude of the  $k$ th harmonic when it passes through frequency  $f_k$ . This reduces to the earlier expression (27) via the substitution  $2\tilde{h}(f) = \sum_k h_{c,k}(f)/f$ . The characteristic amplitude is related to the energy radiated to infinity in each harmonic and is given by

$$h_{c,1} = \frac{5}{\sqrt{672\pi}} \frac{\sqrt{mM}}{r_o} \tilde{\Omega}^{1/6} \mathcal{H}_{c,1}, \quad (\text{A2})$$

$$h_{c,k} = \sqrt{\frac{5(k+1)(k+2)(2k+1)!k^{2k}}{12\pi(k-1)[2^k k!(2k+1)!!]^2}} \times \frac{\sqrt{mM}}{r_o} \tilde{\Omega}^{(2m-5)/6} \mathcal{H}_{c,m} \quad \text{for } m \geq 2. \quad (\text{A3})$$

Here  $\tilde{\Omega} = GM\omega_{orb}/c^3$  is the dimensionless orbital angular frequency and  $r_o$  is the distance to the source. The relativistic correction,  $\mathcal{H}_{c,k}$ , can be written as

$$\mathcal{H}_{c,k} = \sqrt{\mathcal{N} \dot{\mathcal{E}}_{\infty k}}. \quad (\text{A4})$$

In this expression,  $\mathcal{N}$  is the relativistic correction to the number of cycles spent near a particular frequency, and  $\dot{\mathcal{E}}_{\infty k}$  is the relativistic correction to the rate of energy lost to infinity in harmonic  $m$ . These corrections can be computed via integration of the Teukolsky-Sasaki-Nakamura equations and are tabulated in Finn & Thorne (2000). We note that the various corrections are defined relative to their Newtonian values.

Using the results of Finn & Thorne (2000), we can compute the total sky- and orientation-averaged S/N  $\rho_{\text{tot}}$  contributed by the lowest four harmonics of the orbital frequency from the time the source enters the detector band (when  $f_4 = 10\text{Hz}$ ) until plunge, for various spins and masses of the central BH:

$$\rho_{\text{tot}} = \sqrt{\sum_{k=1}^4 \rho_k^2}. \quad (\text{A5})$$

This S/N was used to derive the range formulae presented in § 3.1. We can also compute the leading-order post-Newtonian S/N by including only the quadrupolar  $k = 2$  mode and setting the correction  $\mathcal{H}_{c,2} = 1$ . We find that for  $\chi \lesssim 0.5$  and  $50M_\odot < M < 250M_\odot$ , the post-Newtonian S/N is typically an overestimate by a factor of  $\sim 1.4$ . We note that the data in Finn & Thorne (2000) do not extend to the full range of radii needed for these calculations. Where necessary, we extrapolated their results to larger radius using appropriate power laws. We have verified that the results are insensitive to the exact form of this extrapolation.

The simplest template to use to detect a circular inspiral would include only the dominant, quadrupolar, component of the orbital frequency. It is useful to estimate how much S/N we would lose by ignoring higher harmonics. For circular inspirals in the equatorial plane of a Kerr BH, the fraction of the total energy radiated during an inspiral from infinity that is radiated between a certain Boyer-Lindquist radius  $r_i$  and plunge effectively depends only on the ratio of the initial radius  $r_i$  to the radius of the innermost stable circular orbit,  $r_i/r_{\text{isco}}(\chi)$ , and is otherwise independent of  $\chi$ . Here  $\chi$  is the central BH spin as usual, and  $r_{\text{isco}}$  is the radius of the innermost stable circular orbit, as given in Eq. (17). The energy radiated in higher harmonics of the orbital frequency is suppressed relative to that in the dominant  $k = 2$  harmonic by powers of  $M/r$ . As the BH spin increases,  $r_{\text{isco}}/M \rightarrow 1$  for prograde orbits, and so a larger fraction of the energy is radiated in the regime where  $r \sim M$ . We would therefore expect higher harmonics to contribute most significantly to the total energy flux for prograde inspirals into BHs with large spins. We computed the fraction of the total energy radiated into each harmonic as a function of the BH spin, while the particle inspirals from  $r = 10 r_{\text{isco}}$  to  $r = r_{\text{isco}}$ . This is the range of radii for which Finn & Thorne (2000) tabulate data, and in this range  $\sim 85\%$  of the total energy is radiated in any circular equatorial inspiral. The energy fractions are shown in Figure 5. We see that for  $|\chi| \lesssim 0.3$ , which is the expected IMBH spin range if the IMBH grows via minor mergers,  $\sim 8\%$  of the energy is radiated into harmonics other than the dominant  $k = 2$  harmonic, and most of this energy goes into the  $k = 3$  harmonic.

The contribution of a harmonic to the S/N of a source depends not only on the energy that goes into that harmonic, but also on the shape of the noise curve — higher harmonics enter the detector band earlier, contribute their signal at frequencies where the noise power spectral density is lower, and therefore have an enhanced contribution to the S/N. Figure 6 shows the relative S/N contributed by each harmonic, defined as  $\rho_k/\rho_{\text{tot}}$ , as a function of IMBH mass, for various IMBH spins. Note that this result does not depend on the mass of the inspiraling CO, since we are working in the extreme mass ratio limit. We see that for prograde inspirals, we can lose  $\sim 10 - 25\%$  of the S/N by using templates containing the  $k = 2$  mode only, but this is mostly recovered by including the  $k = 3$  mode in the search templates. (We can lose up to  $\sim 50\%$  of the S/N by using only  $k = 2$  templates

for retrograde inspirals into high-mass IMBHs, but the S/Ns for such events are very small, making their detection unlikely.)

The S/Ns computed from these perturbative waveforms are not totally accurate for the reasons given earlier. Corrections will include finite-mass effects, contributions from the spin of the small BH and the effect of  $k > 4$  harmonics of the orbital frequency. It is clear from Figure 5 that for larger spins, a significant amount of energy goes into harmonics with  $k > 4$ . These harmonics spend even longer in band and so their inclusion would increase the S/N. However, we cannot compute their contribution to the S/N since Finn & Thorne (2000) do not tabulate these contributions separately. Overall, the S/Ns computed here should be accurate to  $\sim 10\%$  and will be more accurate than those computed from the leading-order post-Newtonian waveforms.

## B. Ringdowns

Following the coalescence of an IMBH with a CO, the BH enters the ringdown phase, characterized by oscillations of its quasi-normal modes, particularly the dominant  $l = m = 2$  mode. For IMRIs, the total energy emitted in GWs during the ringdown is  $\sim 0.5m^2/M$  (Flanagan & Hughes 1998), which is a factor of  $O(m/M)$  smaller than the total energy emitted over the inspiral. However, the ringdown GW frequency (Echeverria 1988),

$$f \approx \frac{1}{2\pi M} [1 - 0.63(1 - \chi)^{0.3}], \quad (\text{B1})$$

is higher than the ISCO frequency and is therefore closer to the minimum of the Advanced LIGO noise power spectral density for the typical masses under consideration. For this reason, ringdowns may be detectable by Advanced LIGO despite their lower energy content. This is particularly true if  $m \gtrsim 10 M_\odot$  BHs, rather than NSs, are common as inspiraling companions, since the range for ringdowns scales as  $m^2$  at low redshifts. Moreover, ringdowns will be the only way to detect CO coalescences with slowly-spinning IMBHs with masses above  $350 M_\odot$ , since inspirals into such massive IMBHs will produce GWs at frequencies below the detector low-frequency limit.

The typical Advanced LIGO ringdown-wave ranges (in terms of luminosity distance) as a function of IMBH mass are plotted in Fig. 7 for several choices of inspiraling object mass and IMBH spin. Because some ranges reach out to significant redshifts (up to  $z \sim 0.5$ ), the effect of redshifting is already included in these ranges, unlike in Fig. 3. Redshifting also explains why the range does not scale strictly as  $m^2$ , as high redshifts bring the GW frequency at the detector down into the region where the interferometer is less sensitive.

The astrophysical rate of ringdowns per cluster is greater than or equal to the rate of IMRIs, since every IMRI culminates in a merger and ringdown (but ringdowns could follow coalescences without observable inspirals, i.e., those with direct plunges). The distance sensitivity to ringdowns following inspirals of  $1.4 M_{\odot}$  NSs is probably too low to make them detectable by Advanced LIGO: the total detectable event rate for NS–IMBH ringdowns is  $\sim 20$  times lower than the event rate for NS–IMBH inspirals if the IMBH mass is  $M = 100 M_{\odot}$  and spin is  $\chi = 0.3$ . However, Advanced LIGO will be considerably more sensitive to ringdowns than to inspirals in other mass ranges. For example, ringdowns from  $10 M_{\odot} + 300 M_{\odot}$  coalescences could be detected in a volume  $\sim 200$  times greater than the detection volume for inspirals from these coalescences; if all IMBHs had mass  $M = 300 M_{\odot}$ , and all COs were  $m = 10 M_{\odot}$  BHs with coalescence rate equal to  $\approx 5 \times 10^{-9} \text{ yr}^{-1}$  per cluster as in § 2.1, then the total detectable IMRI ringdown event rate would reach  $\sim 20 \text{ yr}^{-1}$ . Thus, if our expectations about the likely masses involved in IMRIs are incorrect, and coalescences of COs with higher masses with more massive IMBHs are common, searches for ringdown waves can provide a useful back-up to IMRI searches.

## REFERENCES

- Abbott, B., et al. (LIGO Scientific Collaboration). 2008, *Phys. Rev. D*, 77, 062002
- Allen, B., Anderson, W. G., Brady, P. R., Brown, D. A., & Creighton, J. D. E. 2005, arXiv:gr-qc/0509116
- Amaro-Seoane, P., Gair, J. R., Freitag, M., Miller, M. C., Mandel, I., Cutler, C. J. & Babak, S. 2007, *Class. Quantum Grav.*, 24, R113
- Apostolatos, T. A. 1996, *Phys. Rev. D*, 52, 605
- Babak, S. V., Fang, H., Gair, J. R., Glampedakis, K., & Hughes, S. A. 2007, *Phys. Rev. D*, 75, 024005
- Bahcall, J. N., & Wolf, R. A. 1976, *ApJ*, 209, 214
- Baker, J. G., Boggs, W. D., Centrella, J., Kelly, B. J., McWilliams, S. T., Miller, M. C., & van Meter, J. 2007, *ApJ*, submitted (arXiv:astro-ph/0702390)
- Baker, J. G., Centrella, J., Choi, D.-I., Koppitz, M., van Meter, J. R., & Miller, M. C. 2006, *ApJ*, 653, L93
- Bardeen, J. M., Press, W. H., & Teukolsky, S. A. 1972, *ApJ*, 178, 347

- Barish, B. C., & Weiss, R. 1999, *Phys. Today*, 52, 44
- Bekenstein, J. D. 1973, *ApJ*, 183, 657
- Bellazzini, M., Fusi Pecii, F., Montegriffo, P., Messineo, M., Monaco, L. & Rood, R. T. 2002, *Astron. J.*, 123, 1509
- Blanchet, L., Qusailah, M. S. S., & Will, C. M. 2005, *ApJ*, 635, 508
- Brown, D. A., Brink, J., Fang, H., Gair, J. R., Li, C., Lovelace, G., Mandel, I., & Thorne, K. S. 2007, *Phys. Rev. Lett.*, 99, 201102
- Campanelli, M., Lousto, C. O., Zlochower, Y., & Merritt, D. 2007a, *ApJ*, 659, L5
- Campanelli, M., Lousto, C. O., Zlochower, Y., & Merritt, D. 2007b, *Phys. Rev. Lett.*, 98, 231102
- Cutler, C., & Flanagan, E. E. 1994, *Phys. Rev. D*, 49, 2658
- Damour, T., & Gopakumar, A. 2006, *Phys. Rev. D*, 73, 124006
- Ebisuzaki, T., et al. 2001, *ApJ*, 562, L19
- Echeverria, F. 1988, *Phys. Rev. D*, 40, 3194
- Favata, M., Hughes, S. A., & Holz, D. E. 2004, *ApJ*, 607, L5
- Finn, L. S. 1987, *MNRAS*, 227, 265
- Finn, L. S., & Chernoff, D. F. 1993, *Phys. Rev. D*, 47, 2198
- Finn, L. S., & Thorne, K. S. 2000, *Phys. Rev. D*, 62, 124021
- Fitchett, M. J. 1983, *MNRAS*, 203, 1049
- Fitchett, M. J., & Detweiler, S. 1984, *MNRAS*, 211, 933
- Flanagan, E. E., & Hughes, S. A. 1998, *Phys. Rev. D*, 57, 4535
- Flanagan, E. E., & Racine, E. 2007, *Phys. Rev. D*, 75, 044001
- Fregeau, J. M., Larson, S. L., Miller, M. C., O’Shaughnessy, R., & Rasio, F. A. 2006, *ApJ*, 646, L135
- Freitag, M., 2003, *ApJ*, 583, L21

- Freitag, M., Gürkan, M. A., & Rasio, F. A. 2006, MNRAS, 368, 141
- Freitag, M., Rasio, F. A., & Baumgardt, H. 2006, MNRAS, 368, 121
- Friedman, J. L., & Schutz, B. F. 1978, ApJ, 221, 937
- Fritschel, P. 2003, arXiv:gr-qc/0308090
- Fryer, C. L., & Kalogera, V. 2001, ApJ, 554, 548
- Gair, J. R., & Glampedakis, K. 2006, Phys. Rev. D, 73, 064037
- Gonzalez, J. A., Sperhake, U., Bruegmann, B., Hannam, M., & Husa, S. 2007a, Phys. Rev. Lett., 98, 091101
- Gonzalez, J. A., Hannam, M. D., Sperhake, U., Brüggmann, B., & Husa, S. 2007b, Phys. Rev. Lett., 98, 231101
- Gültekin, K., Miller, M. C., & Hamilton, D. P. 2004, ApJ, 616, 221
- Gültekin, K., Miller, M. C., & Hamilton, D. P. 2006, ApJ, 640, 156
- Gürkan, M. A., Fregeau, J. M., & Rasio, F. A. 2006, ApJ, 640, L39
- Gürkan, M. A., Freitag, M., & Rasio, F. A. 2004, ApJ, 604, 632
- Heggie, D. C. 1975, MNRAS, 173, 729
- Heggie, D. C., Trenti, M., & Hut, P. 2006, MNRAS, 368, 677
- Herrmann, F., Hinder, I., Shoemaker, D., & Laguna, P. 2007a, Class. Quantum Grav. , 24, 33
- Herrmann, F., Hinder, I., Shoemaker, D., Laguna, P., & Matzner, R. A. 2007b, ApJ, 661, 430
- Ho, W. C. G. & Lai, D. 1999, MNRAS, 308, 153
- Hopman, C., & Alexander, T. 2005, ApJ, 629, 362
- Hopman, C., & Portegies Zwart, S. F. 2005, MNRAS Lett., 363, L56
- Hopman, C., Portegies Zwart, S. F., & Alexander, T. 2004, ApJ, 604, L101
- Hughes, S. A., & Blandford, R. D. 2003, ApJ, 585, L101

- Hurley, J. R. 2007, MNRAS, 379, 93
- Innanen, K. A., Zheng, J. Q., Mikkola, S., & Valtonen, M. J. 1997. AJ, 113 (5), 1915
- Koppitz, M., Pollney, D., Reisswig, C., Rezzolla, L., Thornburg, J., Diener, P., & Schnetter, E. 2007, arXiv:gr-qc/0701163
- Kozai, Y. 1962, AJ, 67, 591
- Kulkarni, S. R., Hut, P., & McMillan, S. L. W. 1993, Nature, 364, 421
- Madau, P., & Rees, M. J. 2001, ApJ, 551, L27
- Mandel, I. 2007, ApJ, submitted, arXiv:0707.0711
- Martel, K., & Poisson, E. 1999, Phys. Rev. D, 60, 124008
- Miller, M. C. 2002, ApJ, 581, 438
- Miller, M. C., & Colbert, E. J. M. 2004, IJMPD, 13, 1
- Miller, M. C., & Hamilton, D. P. 2002a, MNRAS, 330, 232
- Miller, M. C., & Hamilton, D. P. 2002b, ApJ, 576, 894
- Mouri, H., & Taniguchi, Y. 2002a, ApJ, 566, L17
- Mouri, H., & Taniguchi, Y. 2002b, ApJ, 580, 844
- O’Leary, R., O’Shaughnessy, R., & Rasio, F. A. 2007, PRL, submitted (arXiv:astro-ph/0701887)
- O’Leary, R. M., Rasio, F. A., Fregeau, J. M., Ivanova, N., & O’Shaughnessy, R. 2006, ApJ, 637, 937
- Peres, A. 1962, Phys. Rev., 128, 2471
- Peters, P. C. 1964, Phys. Rev. B, 136, 1224
- Peters, P. C., & Mathews, J. 1963, Phys. Rev., 131, 435
- Phinney, E. S. 1991, ApJ, 380, L17
- Phinney, E. S. 2005, private communication

- Portegies Zwart, S., Baumgardt, H., Hut, P., Makino, J., & McMillan, S. L. W. 2004, *Nature*, 428, 724
- Portegies Zwart, S., & McMillan, S. L. W. 2000, *ApJ*, 528, L17
- Portegies Zwart, S., & McMillan, S. L. W. 2002, *ApJ*, 576, 899
- Press, W. H., & Teukolsky, S. A. 1977, *ApJ*, 213, 183
- Pryor, C., & Meylan, G. 1993, in *Structure and Dynamics of Globular Clusters.*, eds. Djorgovski S. G., Meylan G. (San Francisco: ASP), vol. 50, p. 357
- Quinlan, G. D. 1996, *New Astronomy* 1, 35
- Quinlan, G. D., & Shapiro, S. L. 1987, *ApJ*, 321, 199
- Quinlan, G. D., & Shapiro, S. L. 1989, *ApJ*, 343, 725
- Redmount, I. H., & Rees, M. J. 1989, *Commun. Astrophys.*, 14, 165
- Reisenegger, A., & Goldreich, P. 1992, *ApJ*, 395, 240
- Rubenstein, E. P., & Bailyn, C. D. 1997, *ApJ*, 474, 701
- Sigurdsson, S., & Hernquist L. 1993, *Nature*, 364, 423
- Sopuerta, C. F., Yunes, N., & Laguna, P. 2007, *ApJ*, 656, L9
- Taniguchi, Y., Shioya, Y., Tsuru, T. G., & Ikeuchi, S. 2000, *PASJ*, 52, 533
- Thorne, K. S., in *Three hundred years of gravitation*, edited by S. W. Hawking and W. Israel (Cambridge University Press, Cambridge, 1987), chap. 9, pp. 330–458
- Trenti, M. 2006, arXiv:astro-ph/0612040
- Trenti, M., Ardi, E., Mineshige, S., & Hut, P. 2007, *MNRAS*, 374, 857
- Trenti, M., Heggie, D. C., & Hut, P. 2007, *MNRAS*, 374, 344
- Vallisneri, M. 2000, *Phys. Rev. Lett.*, 84, 3519
- Wainstein, L. A., & Zubakov, V. D. 1962, "Extraction of signals from noise", Prentice-Hall, Englewood Cliffs, NJ
- Wen, L. 2002, *ApJ*, 598, 419

Wiseman, A. G. 1992, Phys. Rev. D, 46, 1517

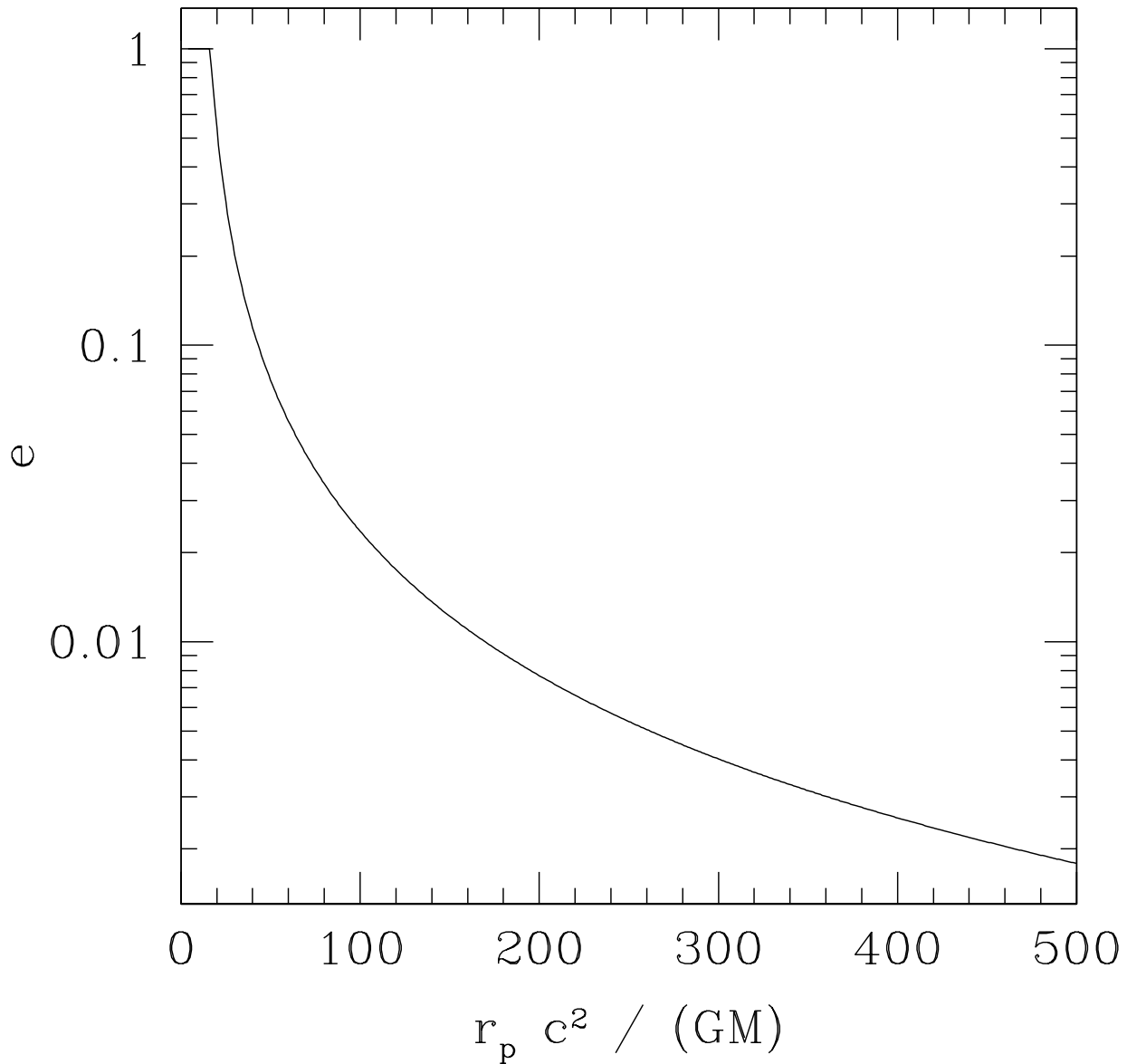


Fig. 1.— Eccentricity at  $f_{\text{GW}} = 10$  Hz as a function of the periapsis at capture, for a CO inspiraling into an IMBH of mass  $M = 100 M_{\odot}$ . The eccentricity at capture is set to 1, and the eccentricity at  $r_p \approx 16 GM/c^2$ , where  $f_{\text{GW}} = 10$  Hz, follows from Eq. (9).

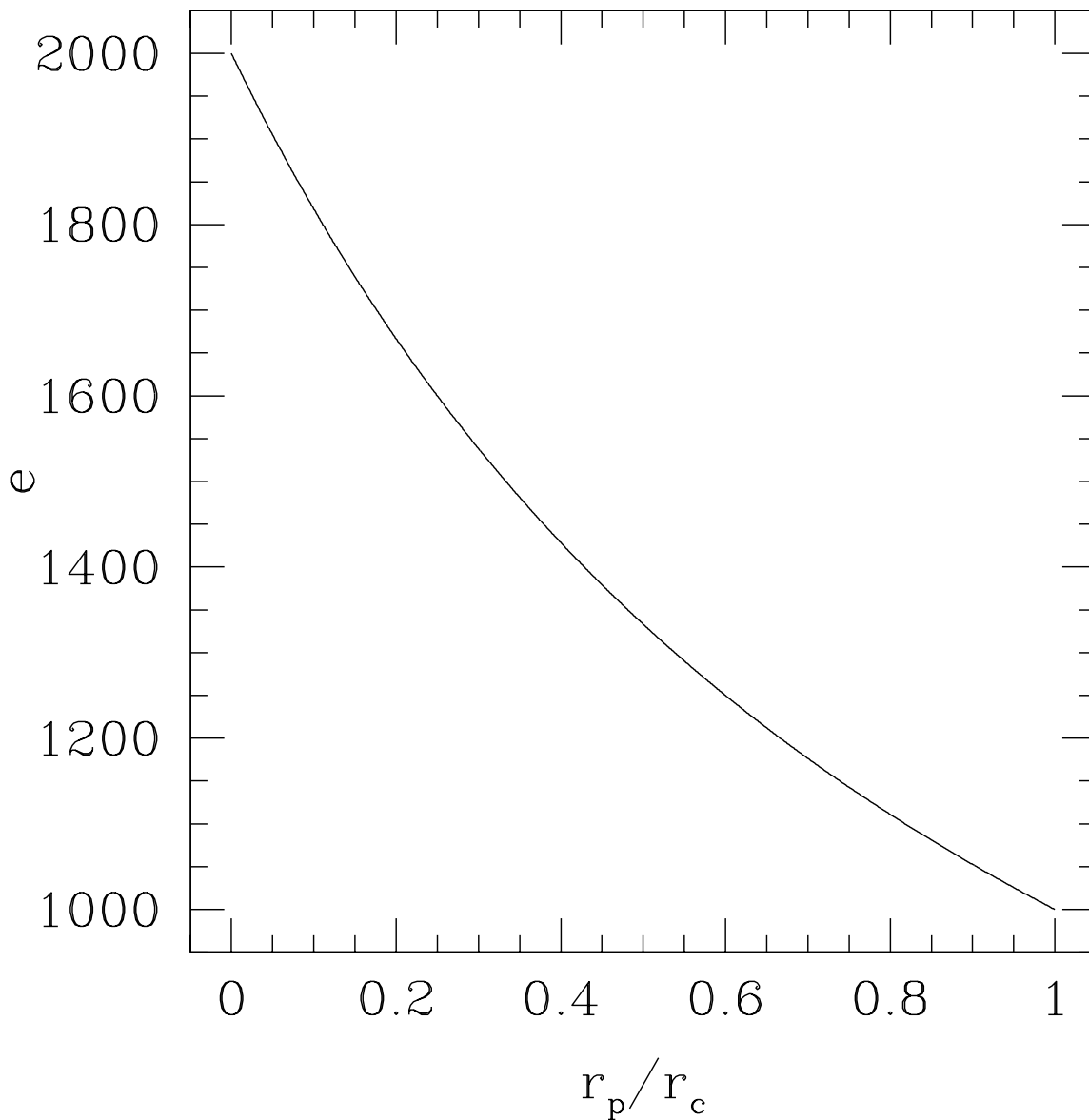


Fig. 2.— Tidal-dissipation-driven inspiral in phase space for an inspiraling star with initial eccentricity of  $e = 1$  and initial periapsis  $r_p = 1000 r_c$ . The plot shows eccentricity on the horizontal axis and the ratio  $r_p/r_c$  on the vertical axis. The radius  $r_c$  characterizes the frequency of normal modes in the star as defined by Eq. (25).

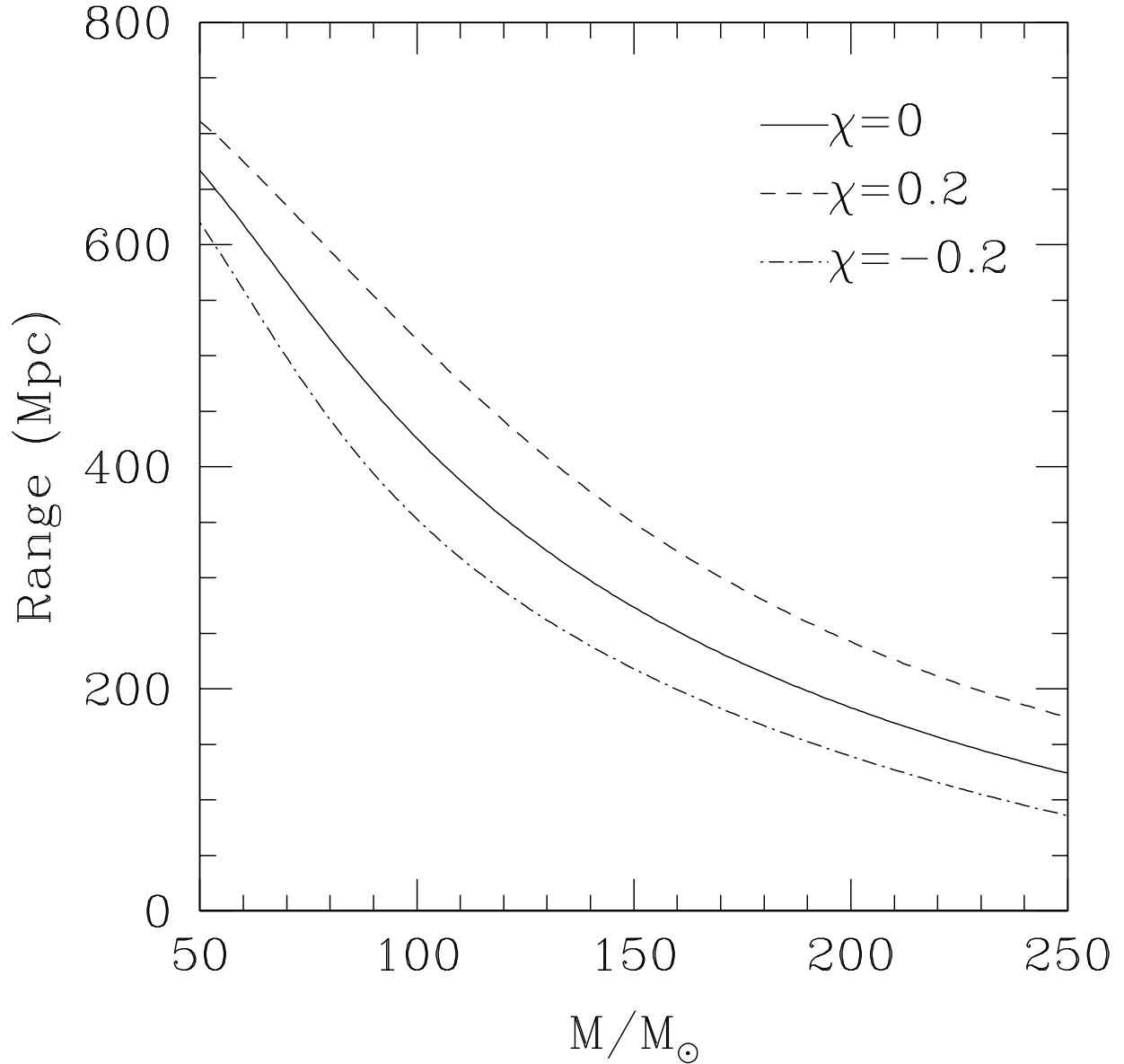


Fig. 3.— Range of a network of three Advanced LIGO detectors for the circular-equatorial-orbit inspiral of a  $1.4 M_{\odot}$  object into an IMBH, as a function of IMBH mass  $M$ . The three lines show IMRI spins of  $\chi = 0.2$  (*dashed*),  $0$  (*solid*), and  $-0.2$  (*dot-dashed*). Positive  $\chi$  means prograde orbit; negative  $\chi$  means retrograde. The quadratic fit given in Eq. (28) is a fit to the  $\chi = 0$  line.

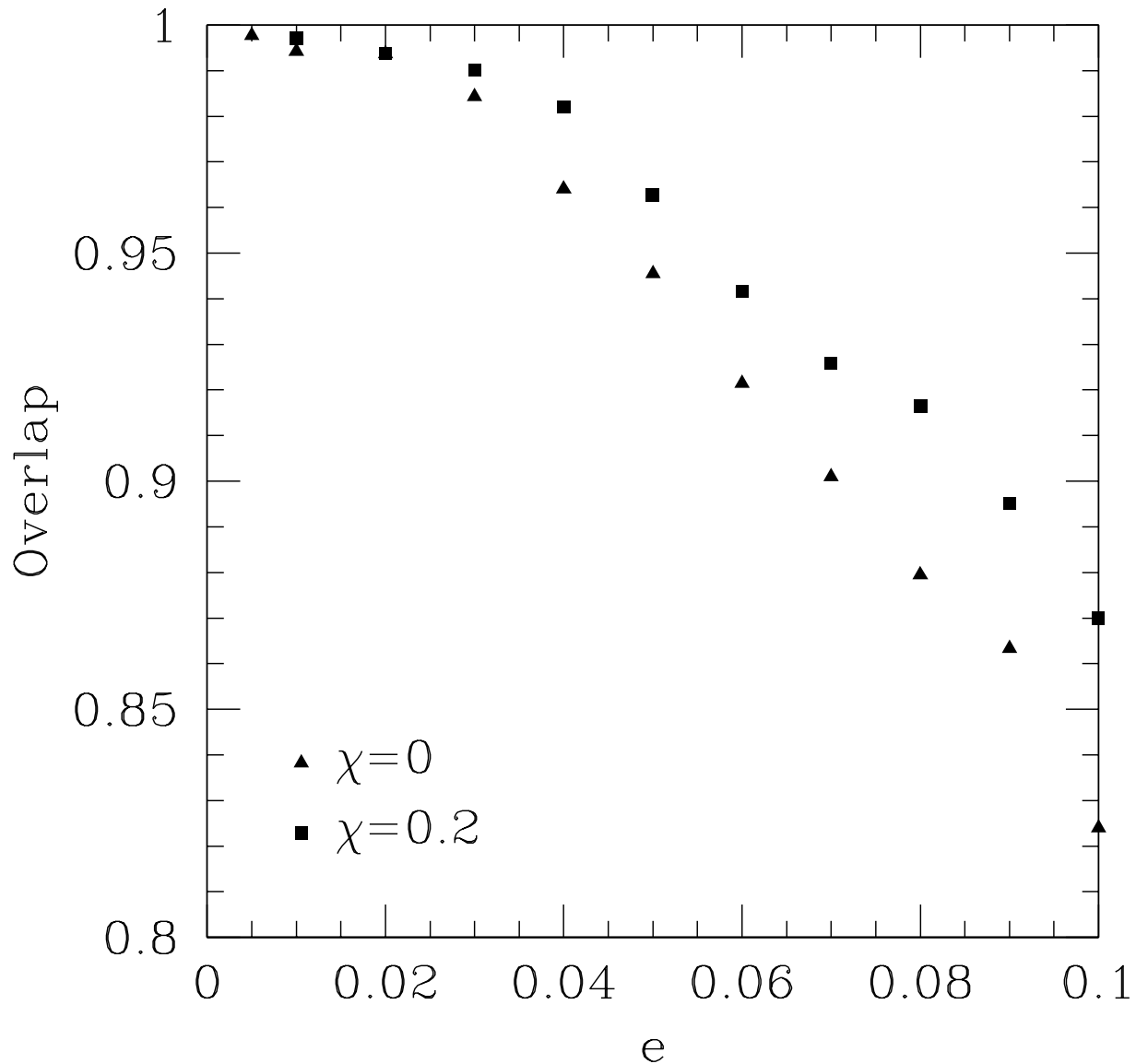


Fig. 4.— Overlaps  $\mathcal{O}$  between a circular template  $h(t)$  and signals  $s(t)$  with varying eccentricities,  $e$ . For both signal and template, the intrinsic parameters  $\vec{\theta} = (M = 100 M_{\odot}, m = 1.4 M_{\odot}, \chi, e)$  are kept constant, with maximization performed only over time of arrival and phase. The overlaps for two values of  $\chi$  are shown.

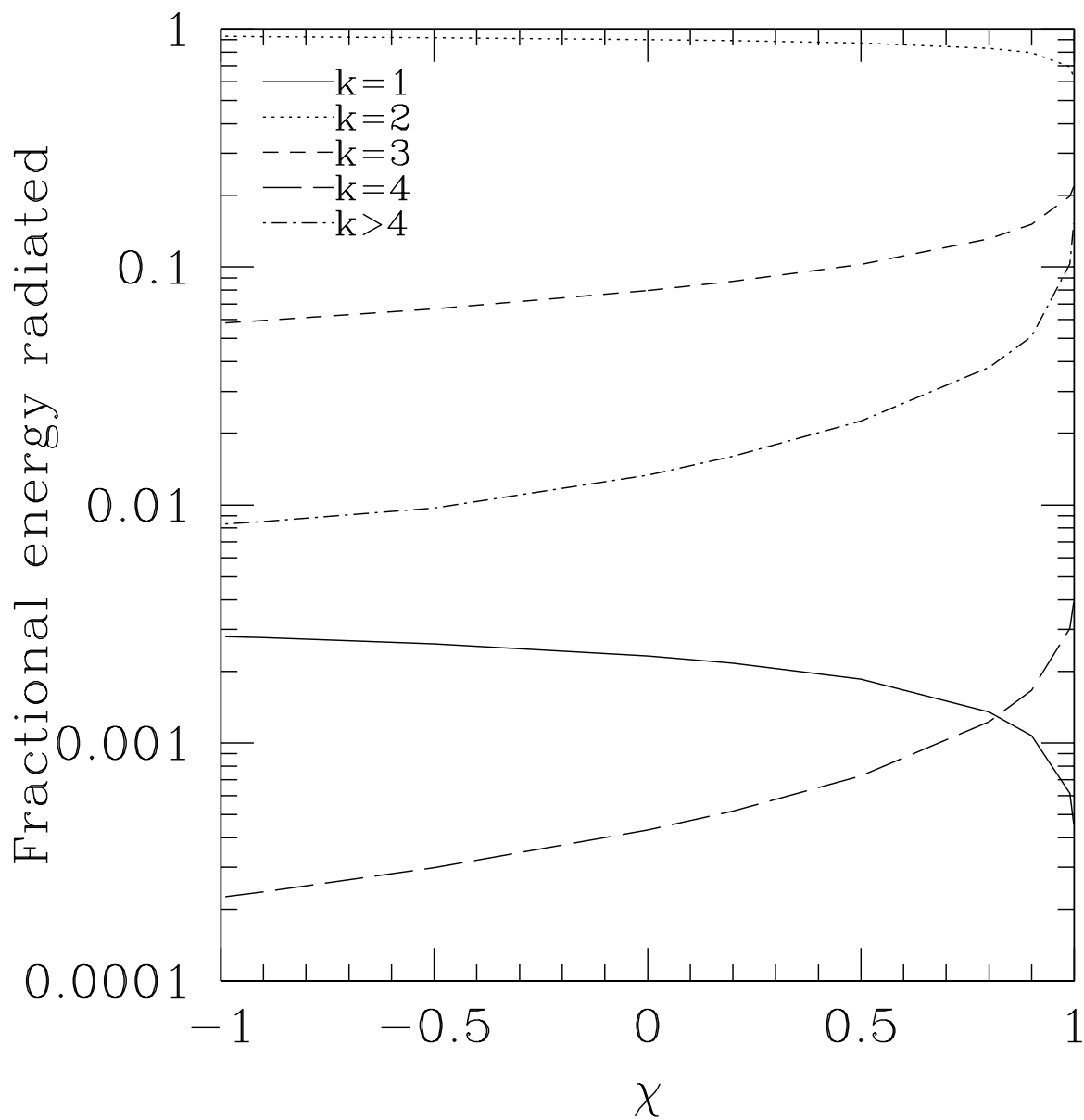


Fig. 5.— Fraction of the total energy radiated into each harmonic of the orbital frequency as the particle inspirals in a circular equatorial orbit from  $10 r_{\text{isco}}$  to  $r_{\text{isco}}$ . This energy fraction is shown as a function of BH spin.

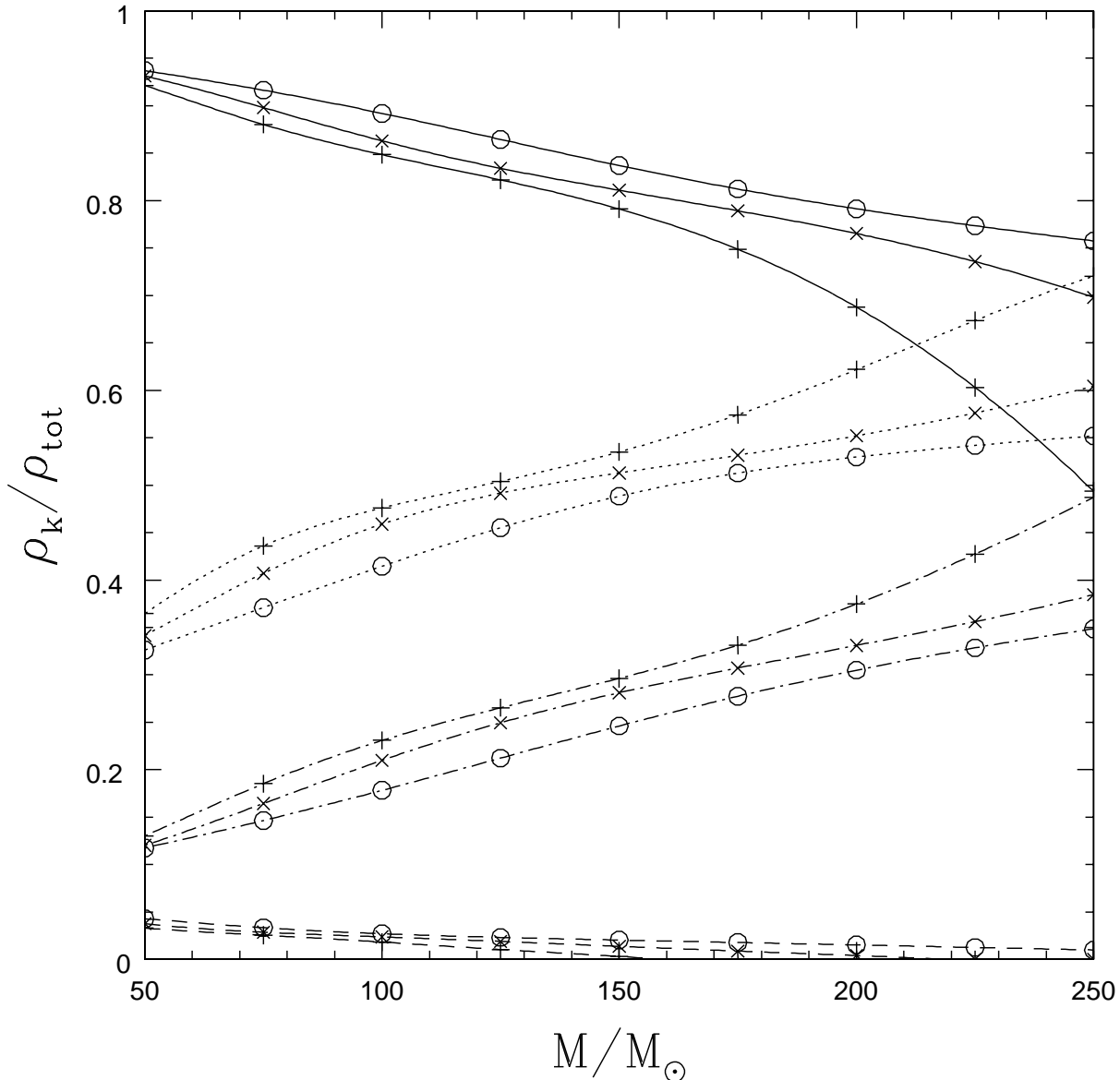


Fig. 6.— Ratio of sky- and orientation-averaged S/N contributed by the lowest four harmonics of the orbital frequency to the total sky- and orientation-averaged S/N contributed by the lowest four harmonics, as a function of the central BH mass, for circular equatorial orbits. The harmonics are indicated by different line styles —  $k = 1$  (*dashed*),  $k = 2$  (*solid*),  $k = 3$  (*dotted*), and  $k = 4$  (*dot-dashed*). Lines are shown for three different BH spins,  $\chi = 0$ ,  $\chi = 0.5$  and  $\chi = -0.5$  (i.e., retrograde inspirals into a  $\chi = 0.5$  BH), indicated by crosses, circles, and plus signs, respectively.

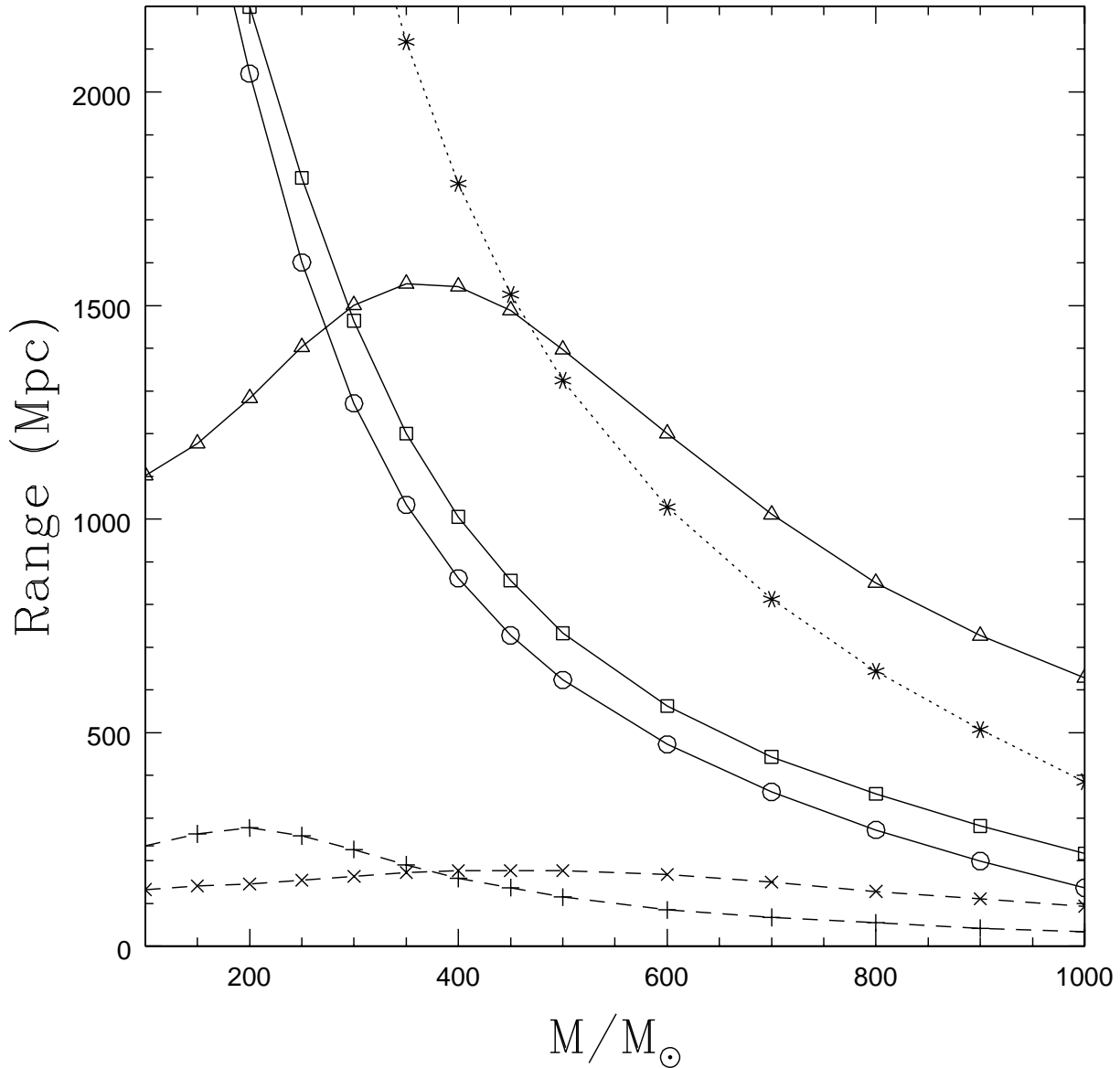


Fig. 7.— Range of a network of three Advanced LIGO detectors for the ringdown of an IMBH following a merger with a CO. The luminosity-distance range in Mpc is plotted as a function of IMBH mass  $M$ ; cosmological redshift is included. Dashed lines denote  $m = 1.4 M_{\odot}$  inspiraling NSs, with plus signs corresponding to IMBH spin  $\chi = 0.3$  and crosses to  $\chi = 1$ . Solid lines denote  $m = 10 M_{\odot}$  inspiraling BHs, with circles, squares, and triangles corresponding to spins  $\chi = 0$ ,  $\chi = 0.3$ , and  $\chi = 1$ , respectively. The dotted line with asterisks denotes  $m = 20 M_{\odot}$  BHs spiraling into an IMBH with spin  $\chi = 0.3$ .